Simulation of Intraplate Stress Distribution of the Indian Tectonic Plate Using the Finite Element Method

ASHISH BAHUGUNA[1] and D. SHANKER[1]

Abstract—The intraplate stress field distribution is estimated by considering the isotropic elastic properties of the Indian plate using numerical analysis. In most modelling, the intraplate stresses are typically established on applying plate-driving forces to a homogeneous elastic plate. However, a tectonic plate comprises continental and oceanic lithosphere with sedimentary basins, cratons, and fold belts with varying significant differences in elastic properties, which likely affect the magnitude and pattern of stress and deformation. In the present study, the finite element method (FEM)-based software packages ABAQUS is used to simulate the intraplate stress distribution in the plate using a 3D mechanical model incorporating the elastic properties of the 19 geological regions of the Indian subcontinent and oceanic region. FEM models are validated with Indian plate fixed GPS velocities and found to be in reasonable agreement with the plate's velocity. This study can augment the interpretability of seismic and geological studies. Also, the model can be helpful to perform seismic hazard assessment (using the stress estimated with the FEM model), identify the seismically active zones and collect insight on active intraplate deformation of seismically active regions of the Indian plate by interpreting the strain rate, deformation rate and stress distribution data.

Keywords: Intraplate stress, ABAQUS, FEM, numerical model, Indian plate, cratons.

1. Introduction

It has been established that the Indian plate has a complex seismotectonic setting, and the distribution of the seismicity is non-uniform and diffuse in the vast region (Sitharam & Kolathayar, 2013). Earthquakes in the NW Himalayan and the NE Himalayan regions are due to interplate activity. In contrast, in the southern Indian Shield, it is primarily due to intraplate activity. Zoback et al. (1989) suggested that most intraplate earthquakes occur due to compressive stress regimes and crustal deformations. However, the relation between the intraplate earthquake cycle and the slow deformation of the plate interiors is still baffling to researchers (Calais et al., 2005), thus presenting significant problems in understanding the related hazards.

The Himalayan region and Northeast region of India are continuously underthrusting beneath the Eurasian plate and Burmese plate, respectively, causing accumulation of high stresses in the Indian plate (Bollinger et al., 2004). Researchers (GSI, 1993; Jain, 1998; Jain et al., 1992; Oldham, 1899; Parvez, 2012; Tiwari, 2010) have reported various historical earthquakes (> Mw 7) in these regions. However, there are different seismic gaps (Garhwal gap, central gap, and Assam gap) identified in the plate, where large earthquake events have not occurred for five centuries (Bilham et al., 2001; Gahalaut, 2008; Khattri, 1987; Singh et al., 1995; Seeber et al., 1981), and paleo-seismological and geodetic findings suggest that strain accumulation is continuing (Jade et al., 2004). Nevertheless, the Himalayan region and Northeast region are considered boundaries of the Indian plate, and these are the most active regions of the plate (Sahu et al., 2006; Sitharam & Kolathayar, 2013). The seismicity map of the Indian plate shows dispersed seismic activity within the plate, which is known as intraplate seismicity. Various significant intraplate earthquake events have occurred in the Indian plate, such as Koyna (M6.6; 1967), Coimbatore (M6.6; 2001), Bhuj (M7.7; 2000), Killari (M6.1; 1993), Satpura (M6.3; 1938), Jabalpur (M6.0; 1997) that have caused immense destruction in the various regions of the Indian subcontinent (Gahalaut, 2010). A number of studies have also provided valuable

[1] Department of Earthquake Engineering IIT, Roorkee, India. E-mail: abahuguna1@eq.iitr.ac.in; d.shanker@eq.iitr.ac.in

insight into the seismicity of the Indian plate through the seismic event catalogue and focal mechanism solution (Bilham & Gaur, 2000; Gahalaut, 2008; Kayal, 2008).

Additionally, various researchers have attempted to study the interplate and intraplate seismicity and the effect of tectonic plate movement on the stress and crustal deformation rate within and at the plate boundaries using finite element method (FEM)-based modelling. Hashimoto (1985) studied the tectonic deformation and stress distribution of Kyushu and surrounding regions of southwestern Japan using a 3D FEM model, the viscosity profiles of the crust and mantle are taken into consideration. Several possible loads, i.e. slab pull, crustal buoyancy, and flows in the asthenosphere, were also used. Similar studies were performed in northeastern Japan by Suito et al. (2002) and Hashimoto and Matsu'ura (2006). Suito et al. (2002) developed a 3D viscoelastic FEM-based kinematic model and established a standard earthquake cycle model by simulating the crustal deformation over the past 100 years. At the same time, Hashimoto and Matsu'ura (2006) proposed a mechanical model of convergent plate boundary zones to simulate the internal stress fields using realistic 3D geometry of the plate interface. Various authors have developed a mechanical model (e.g., Salomon, 2018; Shemenda & Grocholsky, 1992) of the tectonic plate comprising crustal layers and plastic mantle layer. Bird and Liu (1999) published the first global intraplate FEM model to investigate the long-term strain rate in all plate interiors by incorporating the topographic variations and plate boundary faults. Some authors have also considered the material non-linearity (e.g., Liu & Rice, 2005; Liu et al., 2000; Salomon, 2018; Wang et al., 2001; Zhao et al., 2004) by incorporating the viscoelastic properties of the plate, while other researchers have developed a physics-based simulation system (Hashimoto et al., 2014) for the earthquake cycle generation at the plate interface.

Recent numerical models of the Indian plate have been centred on 2D modelling (Cloetingh & Wortel, 1986; Coblentz et al., 1998; DeMets et al.; 2010; Dyksterhuis et al., 2005; Jayalakshmi & Raghukanth, 2015, 2016, 2017; Manglik et al., 2008; Wiens et al., 1985), primarily elastic homogeneous models.

Cloetingh and Wortel (1986) employed five tectonic forces in their model, i.e, ridge push, trench suction force, drag force, slab pull, and resistant force, and estimated a compressive force in the range of 300–500 MPa. Coblentz et al. (1998) investigated the Indo-Australian plate using a 2D FEM model and concluded that by imposing a resistance force along the Himalayan boundary to stabilize the ridge force, the observed stress could be understood without employing basal drag and subduction forces. These studies have provided significant insights into the tectonic forces in the controlling stresses in the Indian plate. However, a number of significant factors have not been addressed by previous studies: (1) Most studies have assumed the Indian plate to be homogeneous rigid. However, recent studies on the Indian lithosphere suggest that it is not homogeneous (Bhukta & Tewari, 2007; Bhukta et al., 2006; Borah et al., 2015; Kilaru et al., 2013; Li & Mashele, 2009; Singh et al., 2004a, 2004b). The geological regions associated with the Indian plate are quite large; hence, their elastic heterogeneity characteristics can influence the spatial change in stress magnitudes and direction. This elastic heterogeneity is not considered in any previous studies of the Indian plate. (2) 2D FEM models have been used in previous studies, and vertical stress is neglected due to the plane stress assumption. (3) Seismic activity is dispersed in the plate, and the origin of these intraplate earthquakes is still obscure due to the drawbacks of the previous 2D models.

In this study, the stress field of the Indian plate is estimated using a 3D FEM model considering the ridge push force, slab pull force, and lateral and vertical inhomogeneity of the geological region. Present studies differ from the previous studies mainly: (1) it is centralized on the Indian plate with a covered area from 34° N–7.6^{o} S to 52° E–100° E (Fig. 1) with an element size of $35 \times 35 \times 10$ km; (2) inhomogeneity of the Indian plate is incorporated that are correlated with the elastic strength parameter of the various geological province such as cratons, traprocks and fold belts. However, the topographic and gravity potential energy difference effect in the local and regional stress fields is not simulated since it requires a comprehensive, detailed structural model of the lithosphere.
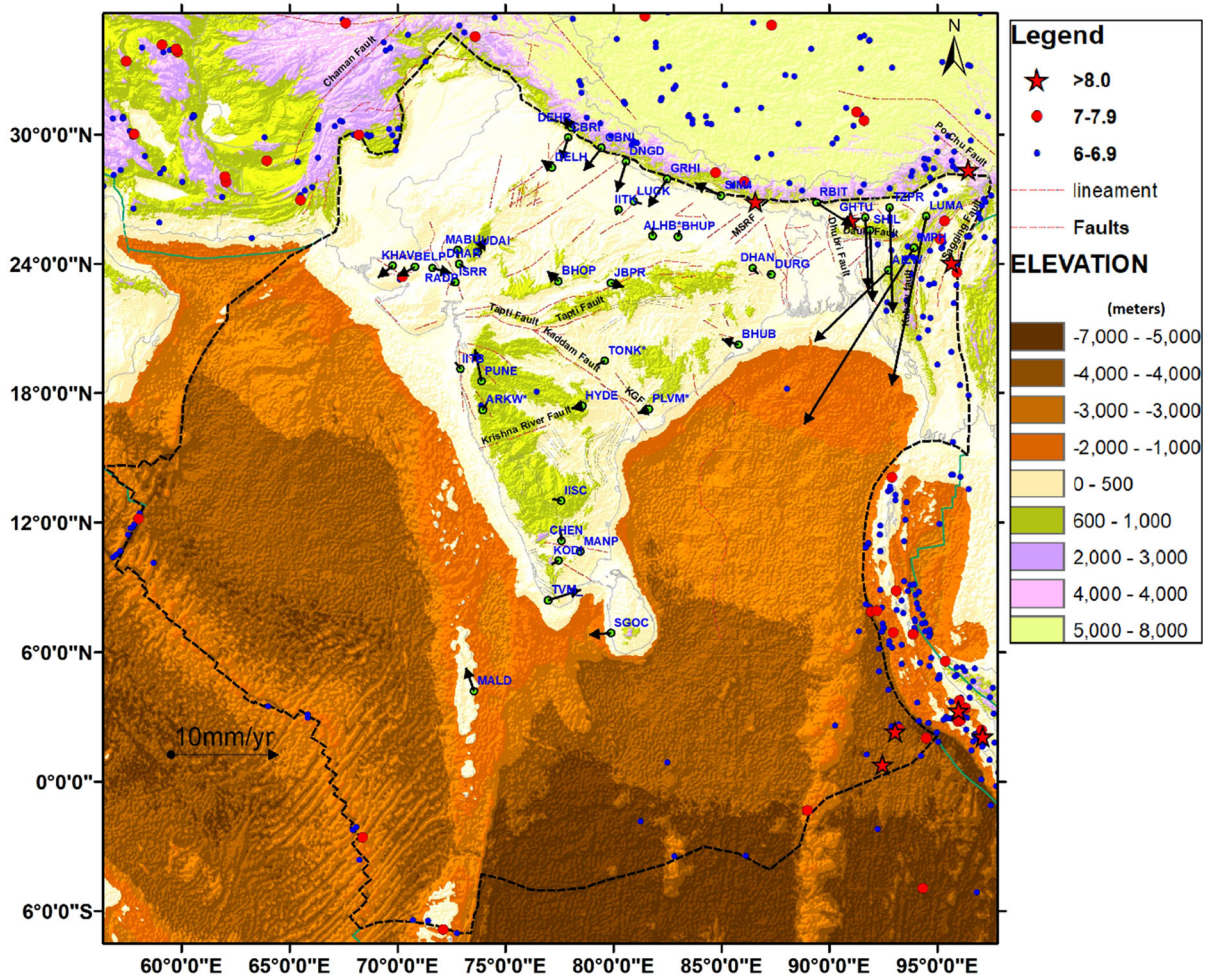
Figure 1
The seismotectonic map (GSI, 2000), the topographic features and seismicity (1900–2019) of the Indian plate are also plotted. Black arrows show the GPS velocity reported by Jade et al. (2017)

2. Geological, Tectonic Setting and Material Properties

The Indian subcontinent is geologically and tectonically intricate. It can be subdivided into various geological regions. These regions have different geological features, tectonic alignment, and evolution history. Figure 2 represents the basic geological units of the Indian subcontinent. Based on the geological map, the Indian plate is divided into 19 significant units. Their features and material properties are discussed below.

2.1. The Himalayan Region

The main geological entities of the Himalayan region are the Tibetan block, Trans-Himalayan, Indus-Tsangpo suture zone (ITSZ), Higher Himalayan crystalline, Lesser Himalayan crystalline, Sub-Himalayan, and the Tethys sedimentary zone (Chatterjee et al., 2013; Gupta & Gahalaut, 2014; Hebert et al., 2012). The south-directed intra-crustal thrust, the Main Central Thrust (MCT), the Main Boundary Thrust (MBT), and the Himalayan Frontal Thrust (HFT) branch out from the Main Himalayan Thrust (MHT). The HFT represents the surface projection of
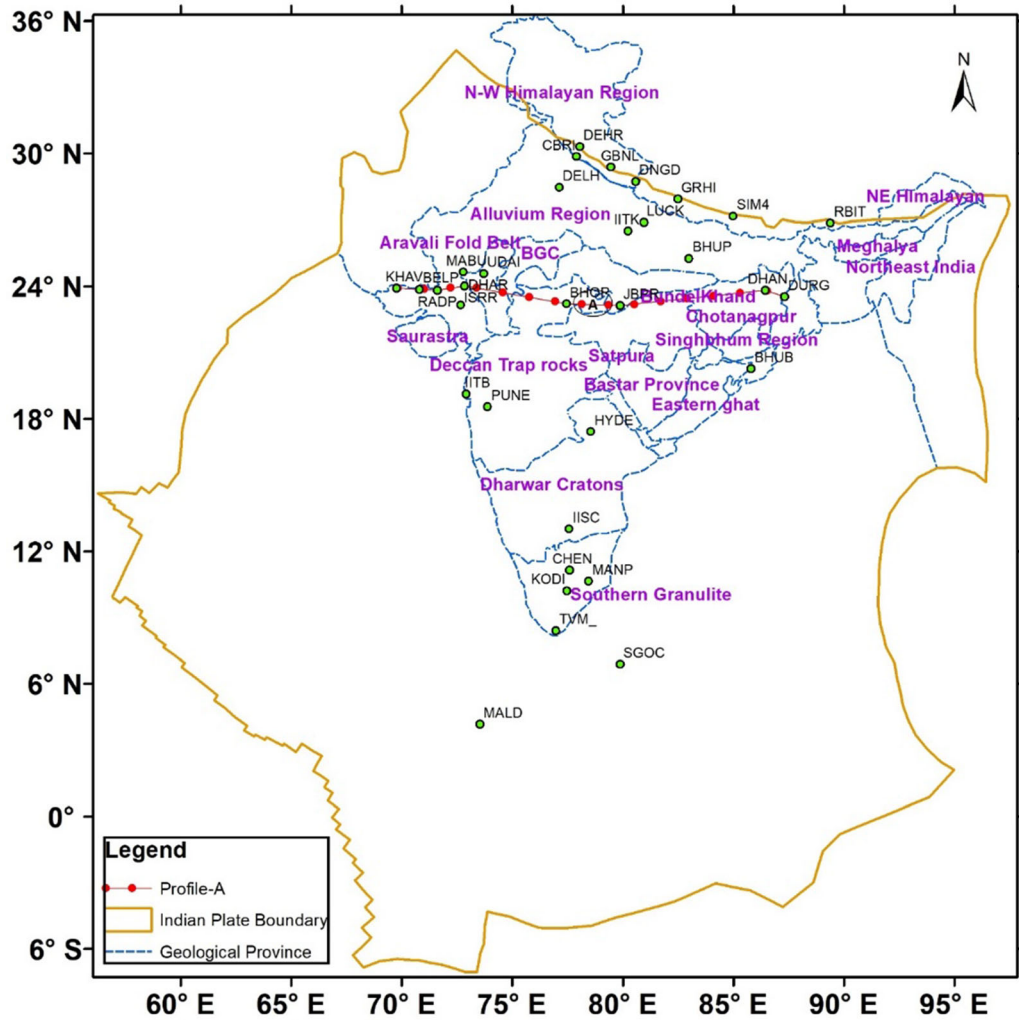
Figure 2
The Indian plate boundary (adopted from Bird, 2003), and geological regions and cratons of the Indian subcontinent (modified after the Geological Map of India)

MHT (Thakur, 2013), and along the HFT, a cluster of intermittent active faulting has been observed (Yeats & Tahakur, 2008), which makes it seismically active (Sahoo, 2012; Thakur, 2013). The MBT demarcates a tectonic boundary between the Lesser Himalayan and Sub-Himalayan. The Lesser Himalayan is separated by the Higher Himalayan along the MCT (Mukul, 2010; Thakur, 2013). Because of the Eurasian and the Indian plate collision, the zone between the MBT and HFT indicates Quaternary deformation in the Himalayan region (Mukul, 2000; Srivastava et al., 2017),

resulting in various earthquake events in the past (Gupta & Gahalaut, 2014).

2.2. Alluvium Region

Sinha et al. (2009) suggested that the Gangetic basin has a cratonic basement, and a similar study by Shau et al. (2015) supports the cratonic basement of the Gangetic Basin adjacent to the Son Valley. It displays N–S thrust faulting in the Siwalik belt along the HFT (Yeats & Tahakur, 2008). There are well-identified faults such as the Great Boundary fault

Table 1

The elastic properties used in the heterogeneous model in this study for the different geological regions of the plates

S. no.	Region	Layer	Density (kg/m³)	Depth (km)	Poisson ratio (μ)	V_s (m/s)	G (Pa) (10^10)	E (Pa) (10^10)	References
1	Western Himalayan region	1	2650	10	0.216	3490.00	3.23	7.85	Li and Mashele (2009); Bhukta et al. (2006); Bhukta and Tewari (2007)
		2	2670	20	0.181	3870.00	4.00	9.44	
		3	2800	30	0.212	3870.00	4.19	10.16	
		4	2900	40	0.260	3870.00	4.34	10.95	
		5 (M)*	3300	> 50	0.287	4480.00	6.62	17.05	
2	Alluvium region	1	2671	10	0.233	3480.00	3.23	8.22	Behera et al. (2004); Borah et al. (2015); Kilaru et al. (2013)
		2	2744	20	0.310	3410.00	3.19	8.22	
		3	2925	30	0.299	3800.00	4.22	10.98	
		4 (M)*	3050	40	0.245	4360.00	5.8	14.43	
		5	3300	> 50	0.291	4400.00	6.39	16.49	
3	BGC region	1	2830	10	0.231	3490.00	3.45	8.49	Julià et al. (2009); Krishna and Rao (2011); Dwivedi et al. (2019)
		2	2890	20	0.274	3850.00	4.28	10.91	
		3	2890	30	0.316	3630.00	3.81	10.02	
		4	2960	40	0.198	4480.00	5.94	14.23	
		5 (M)*	3430	> 50	0.280	4530.00	7.04	18.01	
4	Bundelkhand region	1	2700	10	0.321	3340.00	3.01	7.96	Murty et al. (2004); Julià et al. (2009)
		2	2850	20	0.23	3790.00	4.09	10.07	
		3	2900	30	0.271	3810.00	4.21	10.70	
		4	2900	40	0.143	4390.00	5.59	12.77	
		5 (M)*	3300	> 50	0.273	4600.00	6.98	17.78	
5	Meghalaya region	1	2485	10	0.355	2940.00	2.15	5.82	Rajasekhar and Mishra (2008); Borah et al. (2016)
		2	2810	20	0.235	3480.00	3.4	8.41	
		3	2855	30	0.258	3540.00	3.58	9.00	
		4	2900	40	0.269	3960.00	4.55	11.54	
		5 (M)*	3300	> 50	0.269	4090.00	5.52	14.01	
6	Northeast Province	1	2700	10	0.404	3290.00	2.92	8.21	Kumar et al. (2020); Saikia et al. (2019); Mitra et al. (2018)
		2	2800	20	0.418	3870.00	4.19	11.89	
		3	3240	30	0.431	4550.00	6.71	19.20	
		4	3240	40	0.415	3740.00	4.53	12.82	
		5 (M)*	3240	> 50	0.427	4360.00	6.16	17.58	
7	Burmese region	1	2700	10	0.383	2400.00	1.56	4.30	Kumar et al. (2020); Saikia et al. (2019)
		2	2700	20	0.395	2600.00	1.83	5.09	
		3	2800	30	0.395	3000.00	2.52	7.03	
		4	3100	40	0.413	3600.00	4.02	11.36	
		5 (M)*	3240	> 50	0.413	3800.00	4.68	13.22	

Table 1 *continued*

S. no.	Region	Layer	Density (kg/m³)	Depth (km)	Poisson ratio (μ)	V_s (m/s)	G (Pa) (10¹⁰)	E (Pa) (10¹⁰)	References
8	Bengal Basin	1	2350	10	0.314	2810.00	1.86	4.88	Singh et al., (2016); Rajasekhar and Mishra (2008)
		2	2780	20	0.258	4010.00	4.47	11.24	
		3	2855	30	0.253	3990.00	4.55	11.39	
		4	3200	40	0.273	4480.00	6.42	16.35	
		5 (M)*	3300	> 50	0.269	4500.00	6.68	16.96	
9	Chotanagpur region	1	2630	10	0.262	2954.55	2.3	5.79	Rajasekhar and Mishra (2008); Mandal and Biswas (2016)
		2	2700	20	0.249	3583.82	3.47	8.66	
		3	2800	30	0.249	3699.42	3.83	9.57	
		4	2800	40	0.249	3699.42	3.83	9.57	
		5 (M)*	3300	> 50	0.277	4444.44	6.52	16.65	
10	Singhbhum region	1	2550	10	0.149	3125.00	3.18	7.31	Mandal and Biswas (2016)
		2	2600	20	0.249	3583.82	3.34	8.34	
		3	2750	30	0.253	3757.23	3.84	9.63	
		4	2880	40	0.249	4161.85	4.99	12.46	
		5 (M)*	3300	> 50	0.164	4444.44	8.48	19.75	
11	Eastern Ghats region	1	2600	10	0.262	3300.00	2.83	7.14	Mandal et al. (2015); Mandal and Biswas (2016)
		2	2700	20	0.249	3760.00	3.82	9.54	
		3	2790	30	0.249	4160.00	4.83	12.06	
		4	2880	40	0.249	4160.00	4.98	12.45	
		5 (M)	3300	> 50	0.277	4440.00	6.51	16.61	
12	Satpura region	1	2700	10	0.322	2810.00	2.13	5.64	Murty et al. (2004); Kumar et al. (2015)
		2	2850	20	0.348	3270.00	3.05	8.22	
		3	2900	30	0.367	3580.00	3.72	10.16	
		4	2900	40	0.322	4000.00	4.64	12.26	
		5 (M)*	3300	> 50	0.215	4000.00	5.28	12.83	
13	Aravali region	1	2540	10	0.232	3490.00	3.09	7.62	Julià et al. (2009); Satyavani et al. (2001); Dwivedi et al. (2019)
		2	2900	20	0.225	3740.00	4.06	9.94	
		3	3000	30	0.221	3760.00	4.24	10.36	
		4	3000	40	0.253	4480.00	6.02	15.09	
		5 (M)*	3350	> 50	0.299	4400.00	6.49	16.85	
14	Saurashtra region	1	2590	10	0.226	3800.00	3.75	9.19	Rao and Tewari (2005); Mandal (2006)
		2	2835	20	0.246	4400.00	5.49	13.68	
		3	3000	30	0.305	5040.00	7.62	19.89	
		4 (M)*	3300	> 40	0.207	4970.00	8.15	19.68	
15	Deccan Traps region	1	2680	10	0.280	3276.69	2.88	7.36	Tiwari et al. (2001); Kumar et al. (2020)
		2	2752	20	0.230	3750.16	3.87	9.49	
		3	2900	30	0.300	3415.6	3.38	8.8	
		4 (M)*	3000	40	0.190	5155.53	7.97	18.91	
		5	3275	> 50	0.190	5196.58	8.84	21.05	
16	Bastar region	1	2720	10	0.272	3340.00	3.03	7.72	Rao et al. (2011); Singh and Singh (2019); Kaila et al. (1990)
		2	2720	20	0.311	3790.00	3.91	10.24	
		3	2850	30	0.273	3810.00	4.14	10.53	
		4	2930	40	0.169	4390.00	5.65	13.2	
		5 (M)*	3300	> 50	0.271	4600.00	6.98	17.75	

Table 1 *continued*

S. no.	Region	Layer	Density (kg/m³)	Depth (km)	Poisson ratio (μ)	V_s (m/s)	G (Pa) (10^{10})	E (Pa) (10^{10})	References
17	Dharwar region	1	2720	10	0.258	3462.86	3.27	8.23	Singh et al., (2004a, 2004b); Borah et al. (2014)
		2	2760	20	0.258	3537.14	3.45	8.69	
		3	2890	30	0.277	3750.00	4.06	10.04	
		4	2890	40	0.263	3914.77	4.43	11.12	
		5 (M)*	3300	> 50	0.262	4772.73	7.06	17.82	
18	Southern Granulite region	1	2720	10	0.290	3400.00	3.15	8.11	Rao et al. (2006); Singh et al. (2006); Pathak et al. (2006);
		2	2760	20	0.270	3500.00	3.38	8.61	
		3	2760	30	0.250	3600.00	3.58	8.97	
		4	2960	40	0.240	3650.00	3.94	9.79	
		5 (M)*	3150	> 50	0.290	4400.00	6.10	15.67	
19	Oceanic region	1	2850	10	0.473	2500.00	1.78	5.25	Singh (1988); Singh (1999); Manglik (2002)
		2	3020	20	0.252	3900.00	4.59	15.50	
		3 (M)*	3300	30	0.256	4640.00	7.10	17.84	
		4	3300	40	0.211	4720.00	7.35	17.81	
		5	3300	> 50	0.253	4500.00	6.68	16.74	

Note: (M)* represents the mantle layer

(GBF), Delhi-Moradabad fault, Lucknow fault, West Patna fault, East Patna fault, Monghyr-Saharasa Ridge fault, Malda-Kishanganj fault (Singh et al., 1995; Sinha et al., 2005). Various faults have been identified, such as the NW–SE-trending Kopili fault, NE-SW Brahmaputra fault, and N–S-trending Dhubri fault, which has generated the large earthquakes in 1930 (M7.0). The Kopili fault has experienced two major earthquakes, in 1869 (M7.4) and 1943 (M7.4). Recently, in 2016, an M6.9 earthquake occurred in the SE of the Kopili fault (Gahalaut et al., 2016).

2.3. BGC and Aravali Fold Belt (AFB) Province

The Banded Gneissic Complex (BGC) is part of the Mewar plains in Rajasthan state. The past deformation events have developed NW–SE striking cross faults and folds in this region (Sharma, 2011). However, the AFB has NE and SW trending in the northern and southern parts. AFB extended from Bhilwara to Sawar in the northern part and covered up to Champaner in Gujrat (Heron, 1953). There are various evidential NE-SW faults with strike-slip displacement have identified in this region (Sinha-Roy et al., 1998; Sharma, 2011).

2.4. Bundelkhand Province

Bundelkhand province is also known as the Bundelkhand granite massif or the Bundelkhand granitoid complex (Basu, 1986). The tectonic trend of the Bundelkhand is E–W to ENE–WSW (Sharma, 2011). It has brittle-ductile shear zones, which is a general characteristic of the Bundelkhand region; the elastic parameters are presented in Table 1.

2.5. Satpura Region

The Satpura region, also known as the Satpura Fold Belt (SFB), is composed of Proterozoic rocks. It is considered the southern structural region of the Central Indian Tectonic Zone (CITZ) and strikes E-W to ENE-WSW (Sharma, 2011). The SFB is ∼ 200 km long and ∼ 30 km wide (Narayanaswami et al., 1963; Singh et al., 2004a, 2004b). Granites in the SFB are assumed to have two phases (Bhowmik et al., 1999; Sharma, 2011). Material characteristics are shown in Table 1.

2.6. Meghalaya and Northeast Region

The Meghalaya craton is also called the Shillong-Mikir-Hills Massif; it is an approximately rectangular $\sim 10{,}000$ km^2 area made up of crystalline rocks. Mazumder (1976) revealed that the Meghalaya craton's oldest unit is the Archean Gneissic Complex. The general alignment of the rocks in the Meghalaya craton is E–W to ENE–WSW (GSI, 1973; Sharma, 2011). Evan (1964) concluded that the Shillong plateau moved along the Dauki fault towards the east. There are a number of E–W- and N–S-trending faults in the Meghalaya craton and Northeast region (Bahuguna & Sil, 2020; Dasgupta & Biswas, 2000).

2.7. Burmese Region

The Burmese region is the most seismically active zone in the Indian plate, where the Indian plate is underthrusting beneath the Burmese plate (Gahalaut & Kundu, 2016). The NNW–SSE- to NE–SW-trending Burmese region is extended up to 700 km and has a width of 250 km (Saikia et al., 2019). The average crustal thickness is ~ 43 km (Saikia et al., 2019). There are a number of tectonic domains developed due to E-W directed compressive stresses induced by the subduction process (Baruah et al., 2013). Singh and Shanker (1993) suggested that compressive stresses are acting along the Burmese arc due to the southeast flow of the Tibetan plateau, and this flow is also responsible for the earthquake events in this region.

2.8. Singhbhum Craton (SC)

The Singhbhum craton (SC) of the eastern Indian shield, also called the Singhbhum-Orissa craton, is one of the oldest cratonic regions of the Archean and Proterozoic age in the Indian subcontinent (Mukhopadhyay, 2001; Mukhopadhyay et al., 2008). It is found that SC underthrusted beneath the Chotanagpur Terrain (CT) during 1.6–0.9 Ga (Rekha et al., 2011). The extension of this shear zone is also found along the NW margin of the Singhbhum granite and the southern margin of the Chakradharpur granite (Gupta & Basu, 2000). The mean crustal thickness beneath SC is ~ 43 km (Mandal &

Biswas, 2016). The material properties of the Singhbhum craton are shown in Table 1.

2.9. Chotanagpur Region

The Chotanagpur craton is extended E–W across Chattisgarh, Orissa, Jharkhand, and West Bengal. This craton is made up of mainly granitic genesis and numerous metasedimentary enclaves. The mean crustal thickness beneath Chotanagpur is ~ 41 km using waveform modelling (Mandal & Biswas, 2016). The material characteristics of this region are shown in Table 1.

2.10. Eastern Ghats Belt (EGB)

In this region, the rocks trend NS–SW to NNE–SSW. The western boundary of the EGB with the Dharwar and Bastar cratons is demarcated by suture zones (Gupta et al., 2000; Rao et al., 2011). It is extended over a length of ~ 600 km with a width of 20 km and 100 km in the south and north parts, respectively. The boundary between Singhbhum and EGB is demarcated by Sukinda thrust and shear zones (Sharma, 2011). The mean crustal thickness beneath EGB is ~ 38 km (Mandal & Biswas, 2016). The material characteristics of this region are shown in Table 1.

2.11. Bengal Basin

The Bengal Basin is covered by extensive sediment thickness (> 12 km) (Johnson and Alam, 1991). It is formed during the separation of Antarctica from India in the early Cretaceous (Coffin et al., 2002). Shillong plateau is overthrusting the Bengal Basin from the north, thereby depressing the Sylhet Basin (Najman et al., 2012). The Bengal Basin has experienced two massive earthquakes in the past (1923, M7.0, and 1918 M7.1) (Sharma et al., 2017). Steckler et al. (2016) suggest that soon a large-magnitude earthquake may occur in this region. Rajasekhar and Mishra (2008) and Singh et al. (2016) performed a crustal structure studied in the Bengal Basin and Northeast region of India and revealed various aspects of the crustal characteristics which have been used in this study (Table 1).

2.12. Southern Granulite Region (SGR)

The SGR comprises a mosaic of the Archean/ Proterozoic crustal sections accumulated over the past 3 Ga (Radhakrishna, 1989). SGR is also known as the Pandyan Mobile Belt (Ramakrishnan, 1988; Sharma, 2011). Geological data and Landsat imagery suggest the collision and northward subduction with the Dharwar craton (Drury et al., 1984), which led to late Archean crustal shortening, thickening, and metaphorism of this region. The region has various shear regions, such as the E–W Cauvery fault (Grady, 1971), Moyar shear zone, Bhavani shear zone, and NW–SE-trending Achankovil shear zone (Santosh, 1996). The Cauvery shear zone divides the SGR into two blocks, the southern and northern granulite. The deep seismic reflection studies performed by Rao et al. (2006) and Reddy (2003) have provided the crust's velocity depth model based on refraction/ reflection data and reveal a four-velocity layer. The elastic material properties of the SGR are adopted from Rao et al. (2006), Reddy (2003), Gupta et al. (2003), and Pathak et al. (2006) and are presented in Table 1.

2.13. Dharwar Craton (DC)

The boundary between Dharwar and the SGR is known as the Moyar-Bhavani Shear zone, and the Cuddapah boundary shear zone demarcates the boundary between the DC and Eastern Ghats belts. There are various conspicuous NNW- to N–S-trending shear zones in the DC, such as the Chitradurga, Bababudan, and Balehonnur shear zone (Sharma, 2011). Based on age and lithologies, a N–S shear zone called the Chitradurga Schist Belt (CB) split it into two parts, West Dharwar (WD) and East Dharwar (ED) (Borah et al., 2014; Drury et al., 1984). Receiver function (RF) modelling performed by Borah et al. (2014) reveals a significant variation of Moho depth of 32–38 km in ED and 28–54 km in WD. The average shear wave velocity (Vs) of the crust beneath WD is ∼ 3.85 km/s and ∼ 3.6 km/s in ED. In the present study, the elastic material properties of the Dharwar region is adopted from Borah et al. (2014) and Singh et al., (2004a, 2004b) (Table 1).

2.14. Saurashtra Region

This region is divided into two critical seismic zones (IV and V) of India (BIS, 2002). In this region, various NE–SW-trending faults have been identified (Biswas, 1987). In addition, the region includes fractures associated with the NNW-SSE Dharwar trend, NE-SW Delhi trend, and ENE-WSW Narmada trend, and the region has experienced various significant earthquakes such as the Bhavnagar earthquake (M6, 1910), Paliyad earthquake (M5.7, 1938), Dwarka earthquake (M5,1940), and Talala event (M5, 2007) (Chopra et al., 2012, 2013; Tandon, 1959). The deep seismic sounding (DSS) profile studies of Rao and Tewari (2005) and Mandal (2006) revealed that the upper crust depth is 16 km in the west and 13 km in the east. The Moho is located at a depth of ∼ 36 km in the western part and ∼ 33 km in the eastern part. The elastic material characteristics of this region are presented in Table 1.

2.15. Deccan Traps Region

The Deccan Traps is the northwestern part of southern India; it is considered the most extensive flood basalt in the world (Kumar et al., 2020). It is a seismically active zone of southern India, where the Koyna earthquake event (M6.6 1967) and numerous other events have occurred in the past. Various faults have been identified in this region, such as the west coast fault, Warna fault, Upper Godavari fault, and Krishna River fault, which is demarcated by the southern boundary between Dahrwar and the Deccan Traps. Most of the seismic activity of this region is concentrated between the west coast fault and the Warna fault.

3. Finite Element Modelling of the Indian Plate

Stress accumulation involving activity such as fault rupture or seismic activity are connected with various tectonic forces acting on the tectonic plates, i.e. slab pull, ridge push basal drag, and resistant force. These forces are often difficult to estimate. However, various researchers have reported the magnitude of these forces (Coblentz et al., 1998;

Khan, 2011); among these tectonic forces, ridge push is the only well-known tectonic force that is correlated with the age of the lithosphere (Dyksterhuis et al., 2005; Jayalakshmi & Raghukanth, 2017; Turcotte & Schubert, 2002). Further, to model the Indian plate, the FEM is used, which is widely popular in the research community. It enables using three-dimensional geometries and heterogeneity to develop more accurate and reliable numerical simulations.

The boundary coordinates (latitudes and longitudes) of the Indian plate are obtained from Bird

homogeneous model, μ is 0.25 and E is 0.75GPa for the whole plate (Table 3).

3.1. Linear Elastic Constitutive Model

The linear model can be described as the following,

$$\{\sigma\} = [C]\{\in\} \quad (1)$$

In matrix form,

$$\begin{Bmatrix} \sigma_{11} \\ \sigma_{22} \\ \sigma_{33} \\ \sigma_{12} \\ \sigma_{23} \\ \sigma_{31} \end{Bmatrix} = \frac{E}{(1+\mu)(1-2\mu)} \begin{bmatrix} (1-\mu) & \mu & \mu & & 0 & \\ & (1-\mu) & \mu & & & \\ & & (1-\mu) & & & \\ & & & \frac{(1-2\mu)}{2} & & \\ & Symmetry & & & \frac{(1-2\mu)}{2} & \\ & & & & & \frac{(1-2\mu)}{2} \end{bmatrix} \begin{Bmatrix} \in_{11} \\ \in_{22} \\ \in_{33} \\ \in_{12} \\ \in_{23} \\ \in_{31} \end{Bmatrix} \quad (2)$$

(2003), and based on the geological map of India, the Indian plate is divided into 19 regions (Fig. 2). These regions are formed by the historic collision of Indian and Eurasian plates. In this work, the ABAQUS FEM package is used, which is a widely acknowledged tool in geoscience and engineering research. Figure 3 shows the FEM model of the plate. The size of the model is 5000 km × 4000 km × 100 km, and performing a mesh refinement process, the model is discretized into 400,282 elements and 455,050 nodes. In the FEM model, an eight-node brick element (C3D8R) is used to discretize the geometry (Fig. 3c). All 19 parts of the model are created separately using a Python script after converting the latitude and longitude into the Cartesian coordinate system using Python and connected by tie constraints using the interaction module. In this study, two basic models are developed (Table 2): (1) the homogeneous and (2) the heterogeneous model, with the combined effect of ridge push, collision force, and slab pull force. In the heterogeneous models, each of the 19 parts is divided into five layers, and each of the layers has a different density (ρ), Poisson ratio (μ), and Young's modulus (E), presented in Table 1, whereas in the

The inverse relationship can be written as:

$$\{\in\} = [C^{-1}]\{\sigma\} \quad (3)$$

where $\{\sigma\}$ is stress, $\in$ is strain, vector C is a constitutive matrix, E is Young's modulus, and μ is the Poisson ratio.

The relation between strain vector and nodal displacements in a continuum element can be expressed as,

$$\{\in\} = [B]\{\delta\} \quad (4)$$

where $\{\delta\}$ is a nodal displacement vector and B is a strain displacement transformation matrix. The stiffness matrix of an element can then be expressed as:

$$[K] = \int_V [B]^T [C][B] dv \quad (5)$$

3.2. Boundary Conditions and Tectonic Forces

Various studies (Argus et al., 2011; DeMets et al., 2015; DseMets et al., 2020) have revealed that the Indian plate is moving northward due to various tectonic forces, i.e. ridge push (F_R) at the Indian mid-
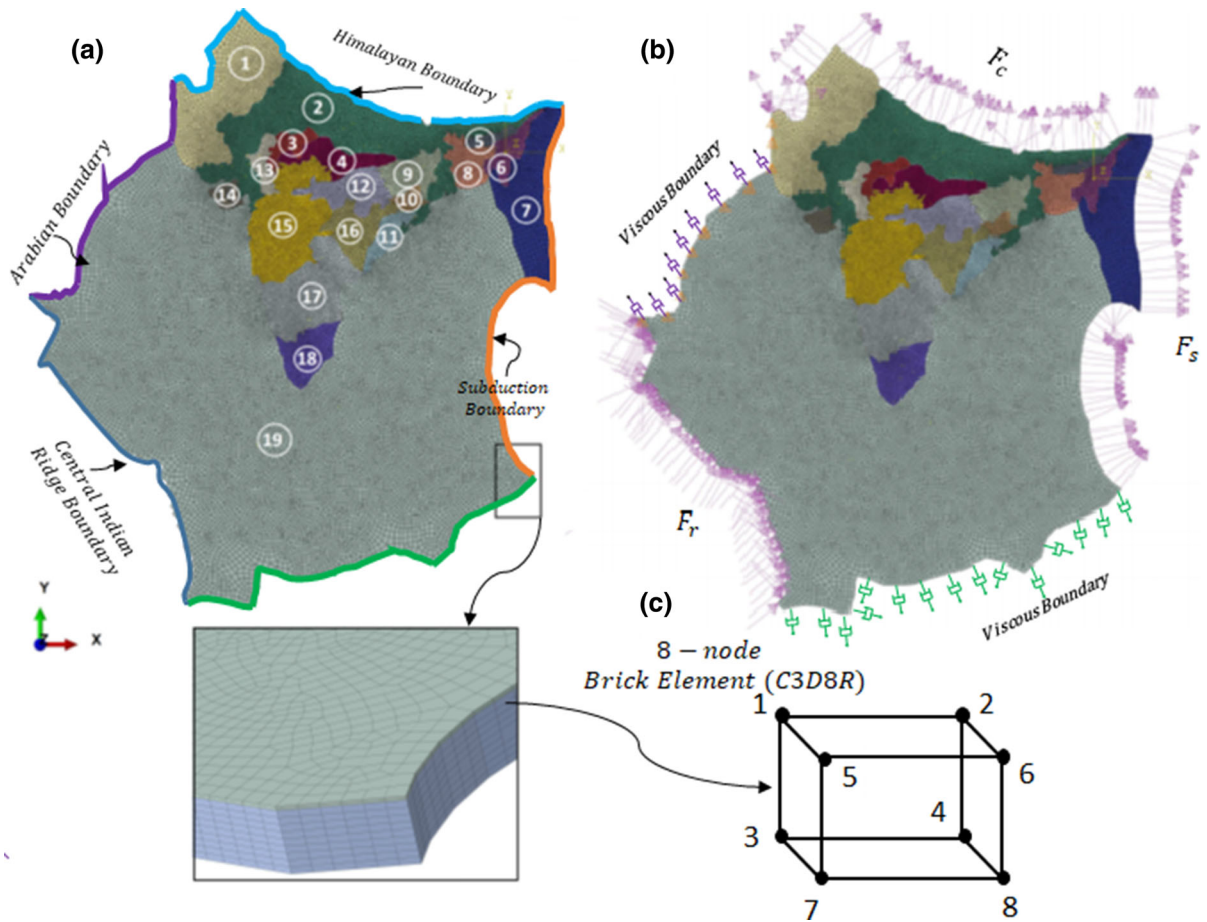
Figure 3
a Finite element model of the Indian plate and its various boundaries. The numbers in circles represent the (1) Western Himalayan, (2) Alluvium region, (3) BGC, (4) Bundelkhand region, (5) Meghalaya region, (6) Northeast region, (7) Burmese region, (8) Bengal Basin, (9) Chotanagpur region, (10) Singhbhum region, (11) Eastern Ghats region, (12) Satpura region, (13) Aravali Fold Belt, (14) Saurashtra region, (15) Deccan Traps, (16) Bastar region, (17) Dharwar region, (18) Southern Granulite region, and (19) Oceanic region. **b** Boundary conditions used in the homogeneous and heterogeneous models. **c** Eight-node brick element used to discretize the models

oceanic region (IMOR), slab pull (F_s) in the subduction region at the Indo-Burmese region (IBR), and collision force (F_C) at the Himalayan boundary. Therefore, these forces are applied in both the homogeneous and heterogeneous models as boundary forces (Fig. 3b). Further, at the Australian and Arabian plate boundary, the non-reflecting boundary (viscous boundary) is applied (Lysmer & Kuhlemeyer, 1969) in the horizontal and vertical directions using the dashpot element at the nodes of the boundaries. The dashpot coefficients are calculated using the following expression:

$$\alpha_h = a\rho v_p x_0 B \qquad (6)$$

$$\alpha_v = b\rho v_s x_0 B \qquad (7)$$

where x_0 and B are the length and width of the element, respectively; $a = b = 1$ are coefficients for maximum absorption; v_p and v_s are P-wave and S-wave velocity of the boundary material, respectively; ρ is the density of the element. Furthermore, to incorporate the mantle resistance at the base of the Indian plate, a dashpot element is introduced. The dashpot element coefficient (c_f) is calculated using the relation given by Turcotte & Schubert (2002):

Table 2

Different models and their boundary conditions used

Boundary	Models	
	Homogeneous	Heterogeneous
Indian mid-oceanic	F_R	F_R
Himalayan boundary	F_C	F_C
Subduction boundary	F_S	F_S
Arabian boundary	Viscous boundary	Viscous boundary
Australian plate boundary	Viscous boundary	Viscous boundary

Table 3

The elastic properties used in the homogeneous model

S. No	Regions		Density (kg/m^3)	Depth (km)	Poisson ratio (μ)	E (GPa)
1	Continental region	Crust	2800	40	0.25	0.75
		Mantle	3300	60	0.25	0.75
2	Oceanic region	Crust	3000	10	0.25	0.75
		Mantle	3300	85	0.25	0.75

$$c_f = \frac{\tau}{v_{avg}} = \frac{-2\eta}{H}\left(2 + 3\frac{h}{H}\right) \qquad (8)$$

where H is the thickness of the upper mantle ($\sim$ 220 km), h is the thickness of the lithosphere ($\sim$ 100 km), v_{avg} is the average plate velocity, η is the viscosity of the upper mantle ranges 10^{19}–10^{20} Pa-s, and τ is shear stress.

The ridge force, which is applied at the Indian mid-oceanic ridge (IMOR) (Fig. 3), is calculated using the expression given by Turcotte & Schubert (2002):

$$F_r = kt(T_m - T_0)\delta\rho_m g\left[2 + \frac{2}{\pi}\frac{\rho_m\delta(T_m - T_0)}{(\rho_m - \rho_w)}\right] \quad (9)$$

where t is the age of the lithosphere in seconds, k is thermal diffusivity (1 mm^2/s), ρ_m is the density of the mantle (3300 kg/m^3), ρ_w is the density of water, g is the acceleration due to gravity, $(T_m - T_0)$ is the temperature difference between mantle and surface (1200 K), and δ is the thermal expansion (3×10^{-5}/K). The magnitude of the force is calculated corresponding to the mean age of the oceanic lithosphere (20 Ma). The collision force (F_C) at the Himalayan boundaries is applied where the Indian plate is converging under the Eurasian Plate. The magnitude of this force is applied as 2×10^{12} N/m, estimated by Coblentz et al. (1998). In contrast, slab pull force (F_S)

along the Indo-Burmese arc is applied as the pressure of magnitude 3.6×10^{13} N/m (Khan, 2011) estimated based on the subduction rate and dip of the subducting slab. This force pulls the plate towards the subduction region. However, estimation of collision and slab pull forces constitute a large amount of uncertainty (Scholz & Campos, 1995).

4. Results and Discussion

4.1. Validation of Models

The developed FEM models are validated with GPS measurement at 33 sites within the Indian subcontinent reported by Jade et al. (2017), shown in Table 4 and Fig. 4. Figure 4a, b shows the comparison of velocity magnitudes obtained and residuals in the respective FEM models relative to GPS data analysis by Jade et al. (2017). It observed that the homogeneous model estimates a maximum residual velocity magnitude of 4.02 mm/year at RBIT station, and at 15 stations (IITK, LUCK, BHUP, MABU, DHAR, ISSR, DHAN, DURG, IITB, HYDE, IISC, KODI, CHEN, MANP, and DHER), the residual velocity magnitude is < 1 mm/year. Similarly, at 11 stations (DELH, KHAV, RADP, BELP, UDAI, BHOP, JBPR, BHUB, SGOC, GBNL, and GRHI),

the residual is in the range of 1–2 mm/year. Similarly, an error range of 2–3 mm/year is estimated at six stations (TVM, PUNE, MALD, CBRI, DNGD, and SIM4). However, with the heterogeneous model, a maximum of 6.02 mm/year is estimated in the residual velocity magnitude at MABU station, and at 12 stations (DELH, KHAV, RADP, BHOP, BHUB, IITB, IISC, KODI, MALD, SGOC, CHEN, and DHER) the residual velocity magnitude is < 1 mm/year. Similarly, at 18 stations (IITK, LUCK, BHUP, BELP, DHAR, ISRR, UDAI, JBPR, DHAN, DURG, PUNE, HYDE, TVM, MANP, CBRI, GBNL, DNGD, and GRHI), the residual is in the range of 1–2 mm/year, and at two stations (SIM4 and RBIT) the residual is in the range of 2–3 mm/year. Overall, it can be seen that out of 33 sites, a total of 30 sites of the heterogeneous model show residuals in the range of 0–2 mm/year, whereas a total of 26 stations in the homogeneous model show residuals in the range of 0–2 mm/year. From Fig. 4b, it is also observed that 91% of the sites in the heterogeneous model show velocity residuals within ± 3 mm/year, and only 9% of sites show residuals of more than ± 3 mm/year, whereas in the homogeneous model, 54.4% of sites show ± 3 mm/year residuals, and 45.6% of sites show residuals of more than ± 3 mm/year, which

Table 4

Comparison of the velocity (mm/year) estimated using the FEM models and Indian plate fixed GPS velocity data

| Stations	Lat	Lon	Homogeneous model				Heterogeneous model				Jade et al. (2017)	
			V_E	σV_E	V_N	σV_N	V_E	σV_E	V_N	σV_N	V_E	V_N
DELH	28.48	77.13	−1.38	0.46	−2.15	2.82	−0.60	0.32	0.72	0.05	−0.92	0.67
IITK	26.51	80.23	0.27	0.53	2.64	3.13	−1.67	1.41	0.06	0.55	−0.26	−0.49
LUCK	26.89	80.94	2.43	1.71	−3.02	2.82	−1.564	2.28	−1.59	1.39	0.72	−0.2
BHUP	25.27	82.99	0.08	0.07	0.17	0.44	−1.43	1.58	0.91	0.29	0.15	0.61
KHAV	23.92	69.77	1.18	2.57	2.46	3.54	−0.78	0.61	0.76	1.84	−1.39	−1.08
RADP	23.82	71.62	0.57	1.16	0.38	0.85	1.96	0.23	0.51	0.98	1.73	−0.47
BELP	23.87	70.8	0.19	1.82	0.66	1.55	0.39	2.02	0.50	1.39	−1.63	−0.89
MABU	24.65	72.78	−1.67	1.72	1.35	2.09	3.16	3.11	6.36	7.12	0.05	−0.75
DHAR	24.01	72.85	0.33	0.32	0.26	0.68	−0.61	1.26	2.28	2.69	0.65	−0.42
ISRR	23.16	72.67	−1.79	1.28	−0.09	0.11	0.86	1.36	1.44	1.64	−0.51	−0.2
UDAI	24.58	73.71	−0.07	0.85	−0.10	1.29	0.08	0.69	2.76	1.57	0.78	1.19
BHOP	23.21	77.45	0.50	1.55	0.62	0.33	0.28	1.33	1.07	0.12	−1.05	0.95
JBPR	23.13	79.88	0.21	0.98	0.00	0.36	−0.69	1.89	2.22	2.58	1.19	−0.36
DHAN	23.82	86.44	2.59	2.07	−0.69	0.13	−1.83	2.35	−0.69	0.14	0.52	−0.56
DURG	23.53	87.31	1.57	2.01	−0.36	0.45	−2.33	1.91	−0.13	0.22	−0.42	0.09
BHUB	20.26	85.79	−0.02	1.52	0.69	0.18	−0.69	0.85	1.72	1.19	−1.54	0.52
IITB	19.13	72.92	−0.56	0.04	−0.23	0.88	0.22	0.74	1.13	0.48	−0.52	0.65
PUNE	18.56	73.88	−0.75	0.15	−0.17	3.14	−0.05	0.55	1.20	1.77	−0.6	2.97
HYDE	17.42	78.55	−2.87	1.88	−0.04	0.21	−1.19	0.21	2.50	2.75	−0.99	−0.25
IISC	13.02	77.57	−0.96	0.12	−0.27	0.45	−0.36	0.48	0.38	0.20	−0.84	0.18
KODI	10.23	77.47	−1.60	0.88	−0.26	0.06	−0.57	0.15	1.69	2.01	−0.72	−0.32
TVM	8.42	76.97	0.76	2.27	−0.83	1.79	−0.58	3.61	1.66	0.69	3.03	0.97
MALD	4.19	73.53	−0.24	0.50	−1.64	3.85	−0.83	0.09	2.18	0.03	−0.74	2.21
SGOC	6.89	79.87	−0.32	1.72	0.72	0.89	−0.23	1.82	1.29	1.47	−2.04	−0.17
CHEN	11.16	77.59	0.14	0.25	−0.47	1.39	−0.34	0.23	1.89	0.96	−0.11	0.93
MANP	10.66	78.46	−0.865	0.97	−0.39	0.87	−0.26	0.36	1.66	1.18	0.1	0.48
DEHR	30.32	78.05	−0.74	0.02	−0.66	1.67	−0.42	0.30	0.60	0.41	−0.72	1.01
CBRI	29.87	77.9	−0.18	0.50	0.84	3.04	−1.08	0.40	−0.03	2.17	−0.68	−2.2
GBNL	29.39	79.45	−0.38	1.26	0.80	2.92	−0.61	1.03	−0.89	1.23	−1.64	−2.12
DNGD	28.75	80.58	−0.65	0.21	−0.04	2.78	−1.09	0.23	−0.29	2.53	−0.86	−2.82
GRHI	27.95	82.49	−0.41	1.36	1.00	3.61	−0.89	0.87	−1.50	1.11	−1.76	−2.61
SIM4	27.17	84.99	−0.28	2.19	−0.24	1.41	−0.07	2.40	−0.43	1.60	−2.47	1.17
RBIT	26.85	89.39	0.11	3.28	1.80	3.99	0.09	3.31	0.18	2.37	3.39	−2.19

(a)

(b)
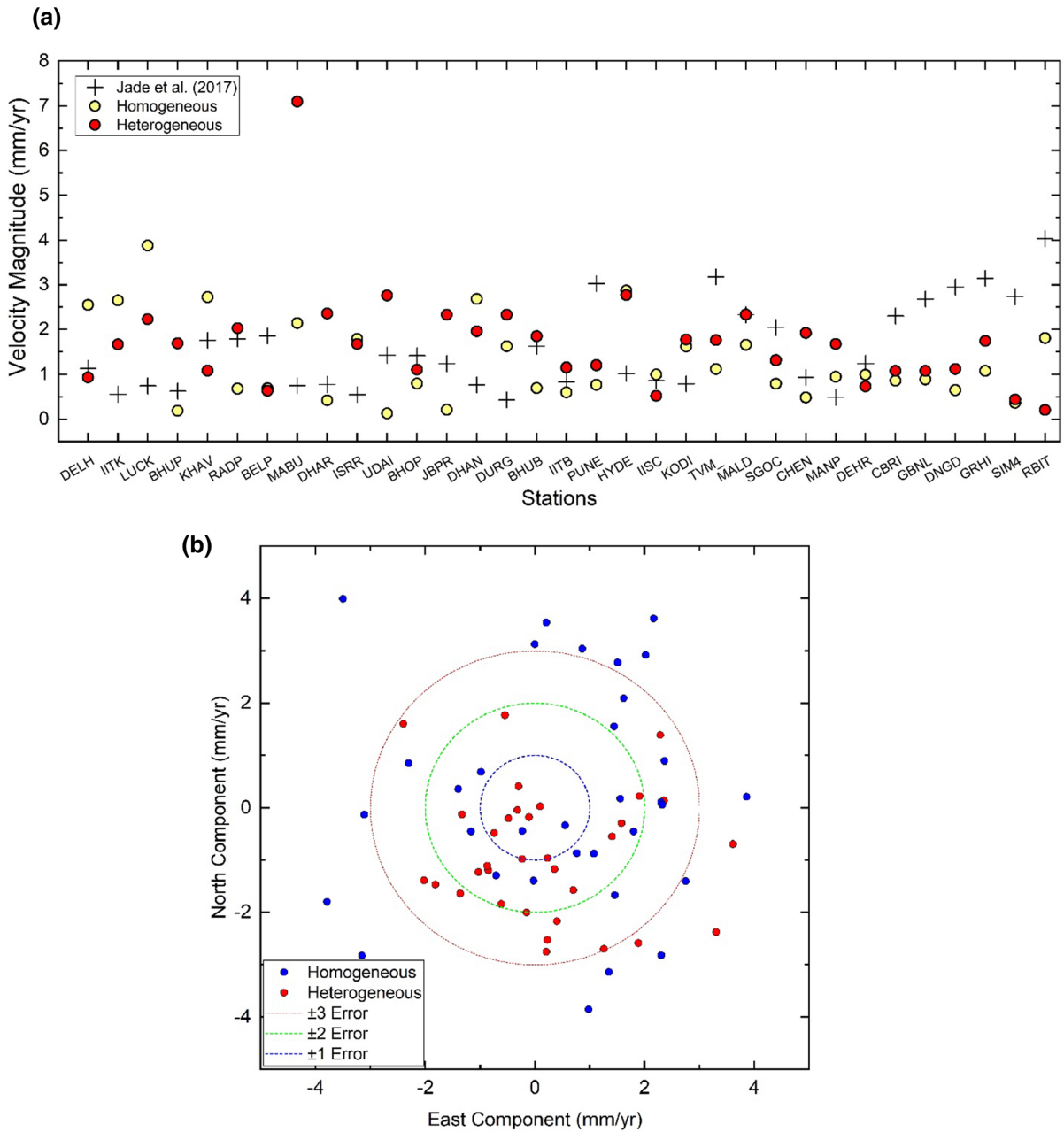
Figure 4

a Comparison of velocity magnitude estimated using FEM homogeneous, heterogeneous and GPS data (Jade et al., 2017). **b** Residual velocity in the north and east component of the homogeneous and heterogeneous models with respect to GPS measurement reported by Jade et al. (2017) is presented in Table 4. Red, green, and violet circles represent the velocity residuals $\pm$ 3, $\pm$ 2, and $\pm$ 1 mm/year, respectively

indicates that the heterogeneous model is more suitable for estimating the stress distribution than the homogeneous model.

Furthermore, the maximum and minimum strain rate obtained using the heterogeneous FEM model at the DHER station is on the order of $\sim 3 \times 10^{-8}$ year^{-1} and -6.45×10^{-8} year^{-1}, respectively, which

Table 5

Strain rate obtained from the best fit heterogeneous-SP model

Regions	Heterogeneous model		Jade et al. (2017)	
	Max. strain rate (year^{-1})	Min. strain rate (year^{-1})	Max. strain rate (year^{-1})	Min. strain rate (year^{-1})
Himalayan region	3.21×10^{-8}	-6.54×10^{-8}	$\sim 4 \times 10^{-10}$	-6×10^{-9}
Alluvium region	2.41×10^{-8}	-6.07×10^{-8}	to	to
BGC	1.67×10^{-8}	-4.82×10^{-8}	6×10^{-9}	2×10^{-9}
Aravalli-Fold Belt	2.25×10^{-8}	-5.57×10^{-8}		
Bundelkhand	2.76×10^{-8}	-5.45×10^{-8}		
Satpura	1.92×10^{-8}	-4.81×10^{-8}		
Singhbhum	1.14×10^{-8}	-5.18×10^{-8}		
Chotanagpur	9.82×10^{-9}	-3.71×10^{-8}		
Eastern Ghats Belt	1.90×10^{-8}	-5.01×10^{-8}		
Bengal Basin	1.12×10^{-8}	-1.96×10^{-8}		
Southern Granulite	2.04×10^{-8}	-6.92×10^{-8}		
Dharwar	1.71×10^{-8}	-5.50×10^{-8}		
Saurashtra	1.1×10^{-8}	-3.67×10^{-8}		
Deccan Traps	1.54×10^{-8}	-4.06×10^{-8}		
Oceanic region	4.42×10^{-8}	-6.97×10^{-8}		

is ~ 10 times lower than the maximum strain rate estimated by Dumka et al. (2018) (4.5×10^{-7} year^{-1}) in most of the Uttarakhand Himalayan region. Similarly, the FEM model estimated the maximum principal strain rate for the Indian subcontinent with a range of 1.1×10^{-8} year^{-1} to 9.82×10^{-9} year^{-1} (tensile) and the minimum principal strain rate with a range of 1.96×10^{-8} year^{-1} (compressive) to 6.97×10^{-8} year^{-1} (compressive), which is ~ 10 times higher than the strain rate reported by Jade et al. (2017) for the Indian subcontinent (Table 5). Also, the strain rate magnitude at the TVM station is estimated at 6.31×10^{-8} year^{-1} (compressive), depicting the shortening in this region, which is ~ 5 times the strain rate reported by Jade et al. (2017) (1.2×10^{-8} year^{-1} (compression)).

Although both the homogeneous and heterogeneous FEM models present reasonably good agreement with the GPS velocity reported by Jade et al. (2017), the strain rates obtained using the FEM models are ~ 10 times lower than those reported by Dumka et al. (2018) and ~ 10 times higher than those reported by Jade et al. (2017). The deviation in the strain rate could be due to the assumptions made for material properties, boundary conditions and constraint applied in FEM modelling. For instance, all 19 geological regions are divided into five layers, and elastic parameters Young's modulus (E) and

Poisson's ratio (μ) are applied as an average value for each layer; the applied average Young's modulus of the layer could be less than the equivalent Young's modulus of the individual layers. However, the strain rate in the model can be controlled by considering more detailed heterogeneous layers of the lithosphere with robust boundary conditions and constraints.

4.2. Effect on Stress Distribution

Figure 5a presents the maximum principal stress, calculated for the heterogeneous and homogeneous models for Profile-A (Fig. 2). A significant difference is observed between the homogeneous and heterogeneous models. For GPS stations KHAV, BELP, RADP, and DHAR, the difference is ~ 75 MPa. However, for GPS stations BHOP, JBPR, DHAN, and DURG, the difference is ~ 20 MPa, and this decrease in stress difference is because to Young's modulus (E) of these regions is almost the same in both the homogeneous and heterogeneous models at the upper crust layer. Similarly, the distortion in normal stress due to heterogeneity is ~ 40 MPa at BELP, DHAN, and DURG; ~ 25 MPa at KHAV, JBPR, DHAR and BHUP; ~ 65 MPa at RADP and ~ 10 MPa at BHOP (Fig. 5b). Figure 5c shows a maximum distortion of ~ 20 MPa in shear stress at DHAR and BHUP and a minimum shear stress
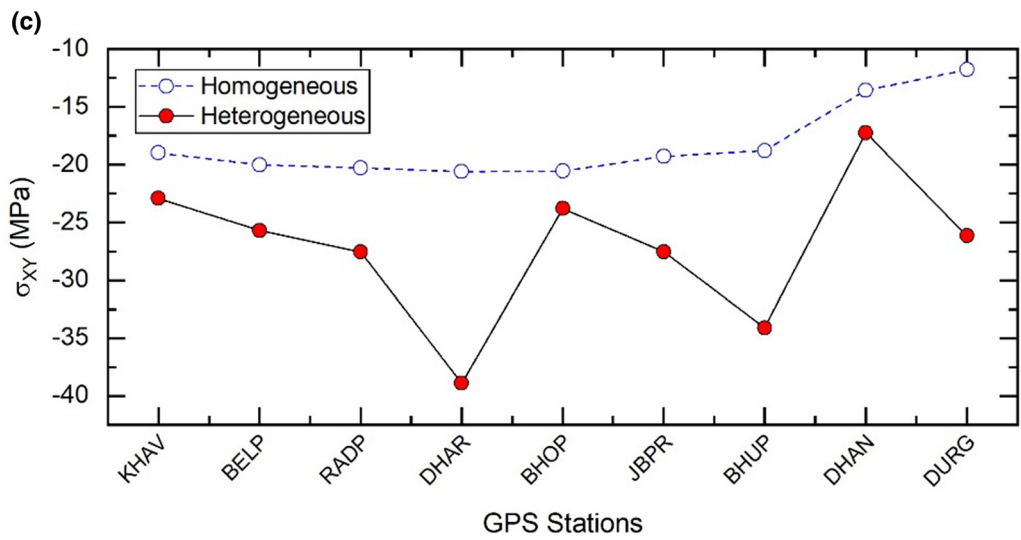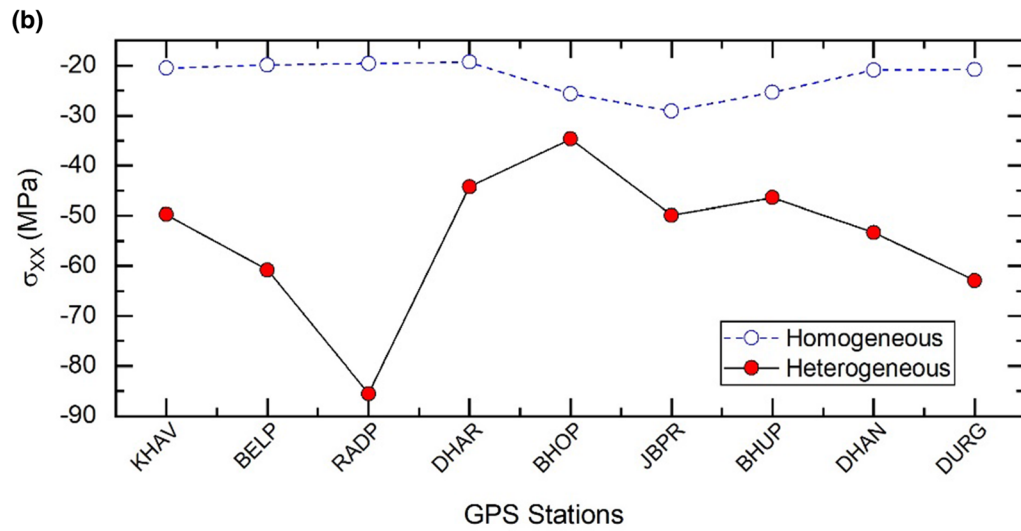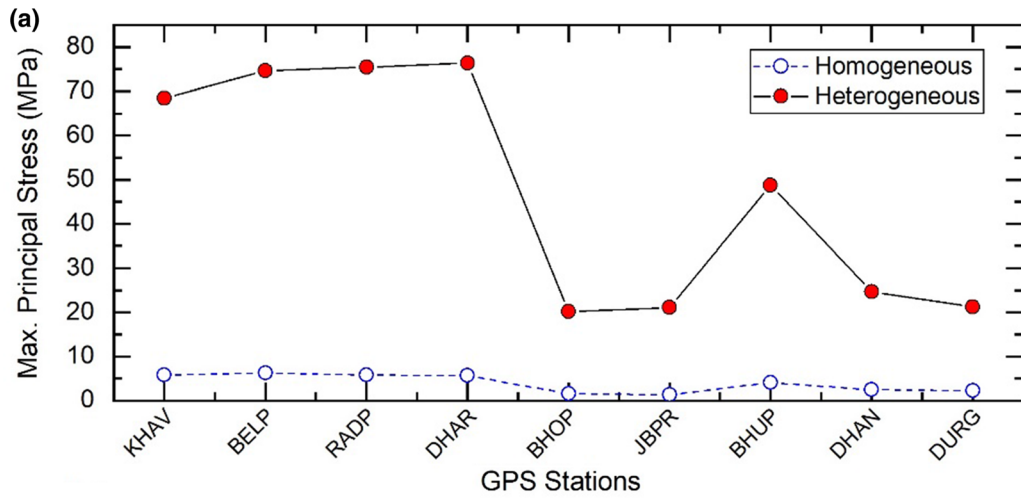
change ∼ 10–15 MPa at KHAV, BELP, RADP, BHOP, JBPR, DHAN and DURG. Perfettin et al. (1999) investigated the triggering effect of Lake Elsman foreshocks (5.3M and 5.4M, 1988–89) on the
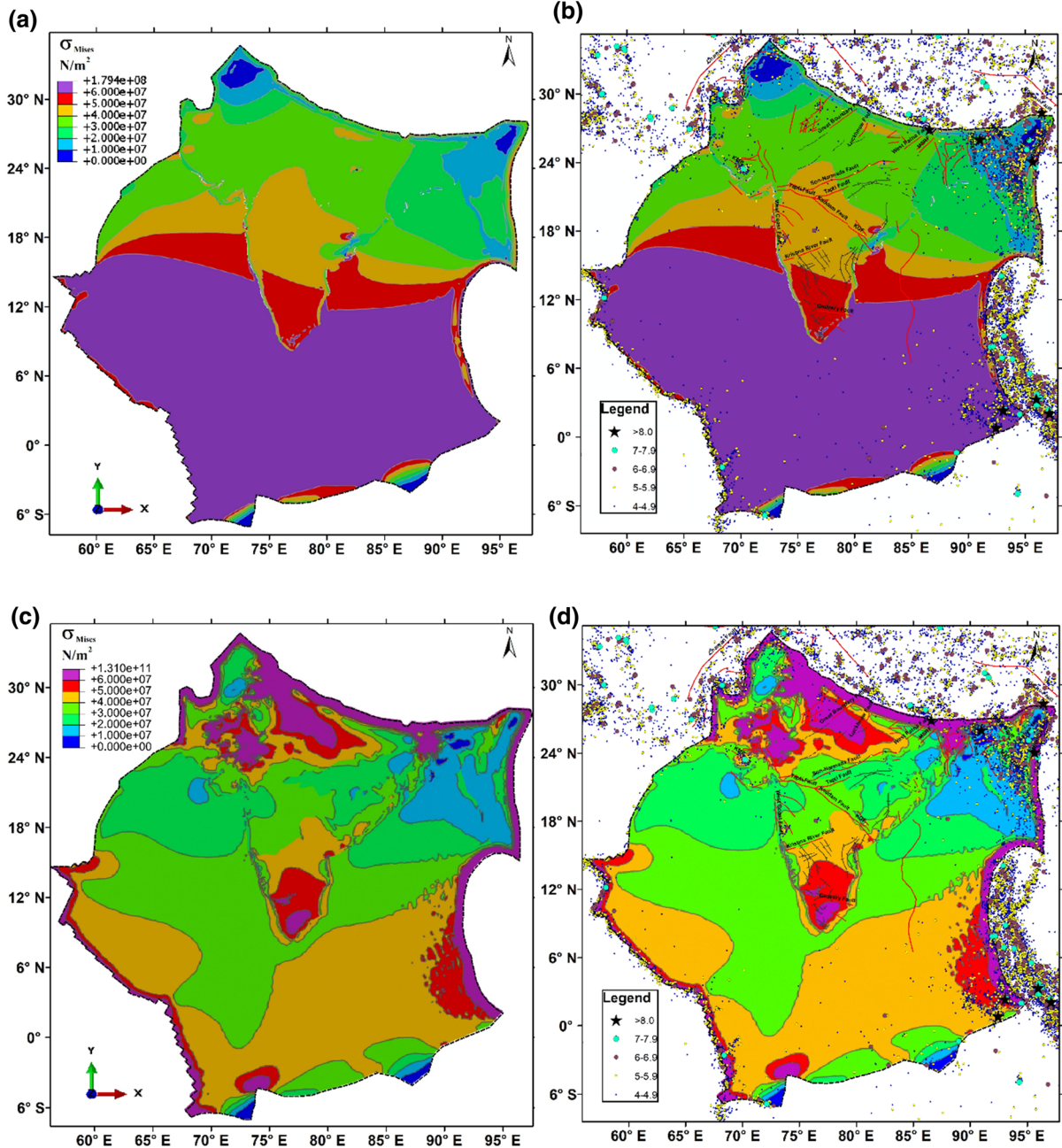

Figure 6
The stress contour obtained from the FEM models and comparison of stress distribution with seismicity of the Indian plate: a, b homogeneous model, c, d heterogeneous model

Loma Prieta earthquake with a homogeneous elastic model and estimated a stress change in the range of 0.03–0.16 MPa. In the present study, the difference observed due to heterogeneity is significant, which is > 100 times the triggering stress (∼ 0.1 MPa) reported by Perfettin et al. (1999). The above results indicate that distortion caused by ignoring the crustal and lateral heterogeneity in stress simulation is significant.

Figure 6 shows the von Mises stress distribution obtained from the homogeneous and heterogeneous models. Figure 6a shows stress obtained with the homogeneous model. It is observed that a high-stress value of magnitude ∼ 180 MPa is estimated in most (70–75%) of the oceanic region and Indo-Burmese region. A stress value of the order ∼ 50–60 MPa can be observed in the southern granulite region, ∼ 40–50 MPa in Dharwar, Deccan Traps, some parts the of Eastern Ghats, Bastar and Satpura regions; similarly, ∼ 20–30 MPa in Singhbhum, Saurashtra, Bundelkhand, Aravali, and Chotanagpur regions, and some parts of the Satpura and Bastar regions. A stress value of ∼ 30–40 MPa is estimated in the Bengal Basin, Meghalaya region, and some parts of the Burmese region and Himalayan region. However, if the stress distribution contour estimated with the homogeneous model is compared with the seismo-tectonic map (Fig. 6b) of the Indian subcontinent, it can be observed that it does not agree, as the homogeneous model (Fig. 6c) estimates a low-stress value in highly seismically active regions such as the Indo-Burmese region, the Himalayan region and the Andaman arc region. At the same time, the hetero-geneous model shows high stress with a magnitude of ∼ 60 MPa–10^5 MPa at the Himalayan plate boundary, Indo-Burmese region, Andaman arc, Indian Mid-Oceanic, and some parts of the Saurashtra and Southern Granulite regions. Similarly, a magni-tude of ∼ 50–60 MPa is observed in the Southern Granulite, and some parts of the Saurashtra, Anda-man arc, Aravali, and Bundelkhand regions. A stress value of ∼ 40–50 MPa is observed in the Deccan Traps, Bundelkhand, and Aravali regions and most of the oceanic region. Stress values in the range of ∼ 30–40 MPa are observed in the Deccan Traps, Eastern Ghats, some parts of the Burmese region and Bastar. Nevertheless, on comparison of stress distribution estimated with the heterogeneous model and seismotectonic features of the Indian subconti-nent (Fig. 6d), it is observed that most of the seismicity and fault ruptures have occurred in the high-stress zones such as the Indo-Burmese region, Andaman arc, and the Himalayan region. Also, the model shows high stress in the Son-Narmada rift valley, where significant earthquakes such as the 1938 Satpura (M6.3), 1927 Son Valley (M6.5), and 1997 Jabalpur (M6.0) have occurred. The model also shows high-stress accumulation near the margin fault, KMF, Krishna river fault and KGE fault, which are also seismically active faults.

Given the effects of lithospheric heterogeneity and stress distribution comparison with seismotec-tonic features, it can be observed that local and regional heterogeneity can affect the location and size of an earthquake. Therefore, it is essential to use realistic heterogeneous characteristics of the litho-sphere in geodetic and seismic studies. In addition, past studies (Harris & Simpson, 1992; Perfettini et al., 1999; Stein et al., 1994) have used stress change to evaluate seismic hazards. In the present study, the average stress difference caused by neglecting the heterogeneity is ∼ 10–20 MPa, which is 100 times larger than the triggering stress (0.1 MPa).

In addition, the heterogeneous model shows close correlation with GPS data and is able to capture the regional stress distribution of the Indian plate. At present, detailed geometrical and rheological data for the intraplate fault are not available and therefore are not incorporated into the present model. However, the faults are the high-stress zones of the tectonic plate where most of the intraplate seismic activity takes place, and incorporating the geometry of the fault would significantly change the local and regional stress distribution of the plate. For instance, Northeast India is considered one of the most seismically active regions in the world due to various inter and intraplate active faults. The present heterogeneous model is able to capture high stress at the boundary of the Burmese region (Fig. 6); however, it fails to capture the high stress in the intraplate regions (Meghalaya and Northeast regions) of Northeast India, which comprises various active faults and thrusts (Fig. 1). Zhao et al. (2004) found that the fault

geometry and faulting type (strike-slip, normal, tensile, and thrusting) can affect the horizontal and vertical deformation by ~ 20–30%, consequently affecting the strain rate. Therefore, neglecting the geometry of the faults can cause an error in interpreting the seismic activity in the region. Also, faulting is a mechanism through which the local and regional stress dropped due to slip in the faults; hence, incorporating the fault geometry in the model, contemporary stresses at the local and regional level can be estimated.

5. Conclusion

In the present study, we attempt to develop a 3D mechanical model of the Indian plate to simulate the stress distribution of the Indian plate with the effect of lithospheric and regional (lateral heterogeneity) heterogeneity. The finite element method is used to estimate the stress and strain distribution of the plate. The model is divided into 19 geological regions, and the effect of the material heterogeneity is studied. Recent available GPS velocity data from Jade et al. (2017) are obtained and compared with simulated velocity at 33 sites. The heterogeneous model is more closely in agreement with GPS measurement than the homogeneous model. We can conclude that it is crucial to incorporate the lithospheric inhomogeneity in geodetic and seismic studies. In addition, in this study, we have neglected the effect of the earth's curvature and local fault characteristics. Therefore, the above conclusions drawn from the effect of heterogeneity on tectonic plate modelling without considering the fault characteristics could be somewhat conservative. Since the difference in stress estimated with the homogeneous and heterogeneous models is much larger, the effect of heterogeneity on stress distribution is highly significant. Further, this analysis can enhance the interpretability of seismic and geological studies. Also, the model can be helpful in performing seismic hazard assessment, identifying seismically active zones, and gaining insight into active intraplate deformation of seismically active regions of the Indian plate by interpreting the strain rate and stress distribution data. However, the linear elastic material assumption is the main limitation of this study. The effect of the rheological models, fault characteristics and other tectonic forces on the Indian plate stress distribution and its seismicity are yet to be explored.

Publisher's Note Springer Nature remains neutral with regard to jurisdictional claims in published maps and institutional affiliations.

REFERENCES

Argus, D. F., Gordon, R. G., & DeMets, C. (2011). Geologically current motion of 56 plates relative to the no-net-rotation reference frame. *Geochemistry, Geophysics, Geosystems*. https://doi.org/10.1029/2011GC003751

Bahuguna, A., & Sil, A. (2020). Comprehensive Seismicity, Seismic Sources and Seismic Hazard Assessment of Assam, North East India. *Journal of Earthquake Engineering, 24*(2), 254–297. https://doi.org/10.1080/13632469.2018.1453405

Baruah, S., Baruah, S., & Kayal, J. R. (2013). State of tectonic stress in Northeast India and adjoining South Asia region. *Bulletin of the Seismological Society of America, 103*, 894–910.

Basu, A. K. (1986). Geology of parts of the Bundelkhand massif, central India. *Geological Survey of India, 117*(2), 61–124.

Behera, L., Sain, K., & Reddy, P. R. (2004). Evidence of underplating from seismic gravity studies in the Mahanadi delta eastern India and its tectonic significance. *Journal of Geophysical Research, 109*(12), 1–25. https://doi.org/10.1029/2003JB002764

Bhowmik, S. K., Pal, T., Roy, A., & Pant, N. C. (1999). Evidence for Pre-Grenville high-pressure granulite metamorphism from the northern margin of the Sausar mobile belt in central India. *Journal of the Geological Society of India, 53*, 385–399.

Bhukta Subrata, K., Sain, K., & Tewari, H. C. (2006). Crustal structure along the Lawrencepur- Astor profile across Nanga Parbat. *Pure and Applied Geophysics, 163*, 1257–1277.

Bhukta Subrata, K., & Tewari, H. C. (2007). Crustal seismic structure in Jammu and Kashmir region. *Journal of the Geological Society of India, 69*, 755–764.

Bilham, R., & Gaur, V. K. (2000). Geodetic contributions to the study of seismotectonics in India. *Current Science, 79*(9), 1259–1269.

Bilham, R., Vinod, K., & Gaur, P. M. (2001). Himalayan Seismic Hazard. *Science, 293*, 1442–1444.

Bird, P. (2003). An updated digital model of plate boundaries. *Geochemistry, Geophysics, Geosystems.* https://doi.org/10.1029/2001GC000252

Bird, P., & Liu, Z. (1999). Global finite-element model makes a small contribution to intraplate seismic hazard estimation. *Bulletin of the Seismological Society of America, 89*(6), 1642–1647.

BIS 1893 (Part 1). (2002). Indian standard criteria for earthquake resistant design of structures, part 1—general provisions and buildings. Bureau of Indian Standards, New Delhi

Biswas, S. K. (1987). Regional tectonic framework, structure and evolution of the western marginal basins of India. *Tectonophysics, 135*, 307–327.

Bollinger, L., Avouac, J. P., Cattin, R., & Pandey, M. R. (2004). Stress buildup in the Himalaya. *Journal of Geophysical Research.* https://doi.org/10.1029/2003JB002911

Borah, K., Bora, D. K., Goyal, A., & Kumar, R. (2016). Crustal structure beneath northeast India inferred from receiver function modeling. *Physics of the Earth and Planetary Interiors, 258*, 15–27.

Borah, K., Kanna, N., Rai, S. S., & Prakasam, K. S. (2015). Sediment thickness beneath the Indo-Gangetic Plain and Siwalik Himalaya inferred from receiver function modelling. *Journal of Asian Earth Sciences, 99*, 41–56. https://doi.org/10.1016/j.jseaes.2014.12.010

Borah, K., Rai, S. S., Priestley, K., & Gaur, V. K. (2014). Complex shallow mantle beneath the Dharwar Craton inferred from Rayleigh wave inversion. *Geophysical Journal International, 198*(2), 1055–1070. https://doi.org/10.1093/gji/ggu185

Calais, E., Mattioli, G., DeMets, C., Nocquet, J. M., Stein, S., Newman, A., & Rydelek, P. (2005). Tectonic strain in plate interiors? *Nature, 438*(7070), E9–E10.

Chatterjee, S., Goswami, A., & Scotese, C. R. (2013). The longest voyage: Tectonic, magmatic, and paleo-climatic evolution of the Indian plate during its northward flight from Gondwana to Asia. *Gondwana Research, 23*(1), 238–267.

Chopra, S., Kumar, D., Rastogi, B., Choudhury, P., & Yadav, R. B. S. (2012). Deterministic seismic scenario for Gujarat region India. *Natural Hazards, 60*, 517–540. https://doi.org/10.1007/s11069-011-0027-y

Chopra, S., Kumar, D., Rastogi, B. K., Choudhury, P., & Yadav, R. B. S. (2013). Estimation of seismic hazard in Gujarat region India. *Natural Hazards, 65*(2), 1157–1178.

Cloetingh, S., & Wortel, R. (1986). Stress in the Indo-Australian plate. *Tectonophysics, 132*(1–3), 49–67. https://doi.org/10.1016/0040-1951(86)90024-7

Coblentz, D. D., Zhou, S., Hillis, R. R., Richardson, R. M., & Sandiford, M. (1998). Topography, boundary forces, and the Indo-Australian intraplate stress field. *Journal of Geophysical Research, 103*(1), 919–931. https://doi.org/10.1029/97jb02381

Coffin, M. F., Pringle, M. S., Duncan, R. A., Gladczenko, T. P., Storey, M., Müller, R. D., & Gahagan, L. A. (2002). Kerguelen hotspot magma output since 130 Ma. *Journal of Petrology, 43*, 1121–1137. https://doi.org/10.1093/petrology/43.7.1121

Dasgupta, A. B., & Biswas, A. K. (2000). *Geology of Assam.* Bangalore: Geological Society of India.

DeMets, C., Gordon, R. G., & Argus, D. F. (2010). Geologically current plate motions. *Geophysical Journal International, 181*(1), 1–80.

DeMets, C., Merkouriev, S., & Jade, S. (2020). High-resolution reconstructions and GPS estimates of India-Eurasia and India-Somalia plate motions: 20 Ma to the present. *Geophysical Journal International, 220*(2), 1149–1171.

DeMets, C., Merkouriev, S., & Sauter, D. (2015). High-resolution estimates of Southwest Indian Ridge plate motions, 20 Ma to present. *Geophysical Journal International, 203*(3), 1495–1527.

Drury, S. A., Harris, N. B., Holt, R. W., Reeves-Smith, G. J., & Wightman, R. T. (1984). Pre-Cambrian tectonics and crustal evolution in south India. *The Journal of Geology, 92*, 3–20.

Dumka, R. K., Kotlia, B. S., Kothyari, G. C., et al. (2018). Detection of high and moderate crustal strain zones in Uttarakhand Himalaya, India. *Acta Geod Geophys, 53*, 503–521. https://doi.org/10.1007/s40328-018-0226-z

Dwivedi, D., Chamoli, A., & Pandey, A. K. (2019). Crustal structure and lateral variations in Moho beneath the Delhi fold belt, NW India: Insight from gravity data modeling and inversion. *Physics of the Earth and Planetary Interiors, 297*, 106317.

Dyksterhuis, S., Albert, R. A., & Müller, R. D. (2005). Finite-element modelling of contemporary and palaeo-intraplate stress using ABAQUS^{TM}. *Computers and Geosciences, 31*(3), 297–307. https://doi.org/10.1016/j.cageo.2004.10.011

Evans, P. (1964). The tectonic frame work of Assam. *Journal of the Geological Society of India, 5*, 80–96.

Gahalaut, V. K. (2008). Major and great earthquakes and seismic gaps in the Himalayan arc. *Memoir Geological Society of India, Golden Jubilee, 66*, 373–393.

Gahalaut, V. K. (2010). Earthquakes in India: hazards, genesis and mitigation measures. *Natural and Anthropogenic Disasters* (pp. 17–43). Springer.

Gahalaut, V. K., & Kundu, B. (2016). The 4 January 2016 Manipur earthquake in the Indo-Burmese wedge, an intra-slab event. *Geomatics, Natural Hazards and Risk, 7*(5), 1506–1512. https://doi.org/10.1080/19475705.2016.1179686

Gahalaut, V., Martin, S., Srinagesh, D., Kapil, S. L., Suresh, G., Saikia, S., Kumar, V., Dadhich, H., Patel, A., Prajapati, S., Shukla, H. P., Gautam, J. L., Baidya, P. R., Mandal, S., & Jain, A. (2016). Seismological, geodetic, macroseismic and historical context of the 2016 Mw 6.7 Tamenglong (Manipur) India earthquake. *Tectonophysics.* https://doi.org/10.1016/j.tecto.2016.09.017

Geological Survey of India. (1973). *Geological and mineral map of Arunachal Pradesh, Assam, Manipur, Meghalaya, Mizoram, Nagaland and Tripura Nagaland and Tripura.* GSI.

Grady, J. C. (1971). Deep main faults of south India. *Journal of the Geological Society of India, 12*, 56–62.

GSI. (1993). *Geological map of India.* Published by Geological Survey of India.

GSI. (2000). *Seismotectonic Atlas of India and Its Environs," Geological Survey of India, Bangalore, India.* GSI.

Gupta, A., & Basu, A. (2000). North Singhbhum Proterozoic mobile belt, eastern India—a review. *Geological Society of India Special Publications, 55*, 195–226.

Gupta, H., & Gahalaut, V. K. (2014). Seismotectonics and large earthquake generation in the Himalayan region. *Gondwana Research, 25*(1), 204–213.

Gupta, S., Bhattacharya, A., Raith, M., & Nanda, J. K. (2000). Contrasting pressure-temperature deformation history across a vestigial craton–mobile belt boundary: The western margin of the Eastern Ghats Belt at Deobhog India. *Journal of*

Metamorphic Geology, 18, 683–697. https://doi.org/10.1046/j.1525-1314.2000.00288.x

Gupta, S., Rai, S. S., Prakasam, K. S., Srinagesh, D., Bansal, B. K., Chadha, R. K., & Gaur, V. K. (2003). The nature of the crust in southern India: Implications for Precambrian crustal evolution. *Geophysical Research Letters, 30*(8), 1–4. https://doi.org/10.1029/2002GL016770

Harris, R. A., & Simpson, R. W. (1992). Changes in static stress on southern California faults after the 1992 Landers earthquake. *Nature, 360*(6401), 251–254. https://doi.org/10.1038/360251a0

Hashimoto, C., Fukuyama, E., & Matsu'ura, M. (2014). Physics-based 3-D simulation for earthquake generation cycles at plate interfaces in subduction zones. *Pure and Applied Geophysics, 171*(8), 1705–1728. https://doi.org/10.1007/s00024-013-0716-4

Hashimoto, C., & Matsu'ura, M. (2006). 3-D simulation of tectonic loading at convergent plate boundary zones: Internal stress fields in northeast Japan. *Pure and Applied Geophysics, 163*(9), 1803–1817. https://doi.org/10.1007/s00024-006-0098-y

Hashimoto, M. (1985). Finite element modeling of the three-dimensional tectonic flow and stress field beneath the Kyushu island, Japan. *Journal of Physics of the Earth, 33*(3), 191–226.

Hébert, R., Bezard, R., Guilmette, C., Dostal, J., Wang, C. S., & Liu, Z. F. (2012). The Indus-Yarlung Zangbo ophiolites from Nanga Parbat to Namche Barwa syntaxes, southern Tibet: First synthesis of petrology, geochemistry, and geochronology with incidences on geodynamic reconstructions of Neo-Tethys. *Gondwana Research, 22*(2), 377–397.

Heron, A. M. (1953). The Geology of Central Rajputana. *Geological Society of India, 79*, 389.

Jade, S., Bhatt, B. C., Yang, Z., Bendick, R., Gaur, K., Molnar, P., Anand, M. B., & Kumar, D. (2004). Preliminary tests of plate-like or continuous deformation in Tibet. *Geological Society of America Bulletin, 116*, 1385–1391.

Jade, S., Shrungeshwara, T. S., Kumar, K., Choudhury, P., Dumka, R. K., & Bhu, H. (2017). India plate angular velocity and contemporary deformation rates from continuous GPS measurements from 1996 to 2015. *Scientific Reports, 7*(1), 1–16.

Jain, S. K., Singh, R. P., Gupta, V. K., & Nagar, A. (1992). Garhwal Earthquake of October 20, 1991. *EERI Special Repor, EERI Newsletter, 26*(2), 1–4.

Jain, S. K. (1998). Indian Earthquake: An Overview. *The Indian Concrete Journal, 72*, 11.

Jayalakshmi, S., & Raghukanth, S. T. G. (2015). An engineering model for seismicity of India. *Geomatics, Natural Hazards and Risk, 6*(1), 1–20. https://doi.org/10.1080/19475705.2013.815282

Jayalakshmi, S., & Raghukanth, S. T. G. (2016). Intra plate stresses using finite element modelling. *Acta Geophysica, 64*(5), 1370–1390. https://doi.org/10.1515/acgeo-2016-0050

Jayalakshmi, S., & Raghukanth, S. T. G. (2017). Finite element models to represent seismic activity of the Indian plate. *Geoscience Frontiers, 8*(1), 81–91. https://doi.org/10.1016/j.gsf.2015.12.004

Johnson, S. Y., & Alam, A. M. N. (1991). Sedimentation and tectonics of the Sylhet trough, Bangladesh. *Geological Society of America Bulletin, 103*(11), 1513–1527. https://doi.org/10.1130/0016-7606(1991)103%3c1513:SATOTS%3e2.3.CO;2

Julià, J., Jagadeesh, S., Rai, S. S., & Owens, T. J. (2009). Deep crustal structure of the Indian shield from joint inversion of P wave receiver functions and Rayleigh wave group velocities: Implications for Precambrian crustal evolution. *Journal of*

Geophysical Research, 114(10), 1–25. https://doi.org/10.1029/2008JB006261

Kaila, K. L., Murty, P. R. K., Rao, V. K., & Venkateswarlu, N. (1990). Deep Seismic sounding in the Godavari Graben and Godavari (coastal) Basin India. *Tectonophysics, 173*(1–4), 307–317. https://doi.org/10.1016/0040-1951(90)90226-X

Kayal, J. R. (2008). *Microearthquake seismology and seismotectonics of South Asia.* Springer Science & Business Media. https://doi.org/10.1007/978-1-4020-8180-4

Khan, P. (2011). Role of unbalanced slab resistive force in the 2004 off Sumatra mega earthquake (Mw > 9.0) event. *International Journal of Earth Sciences, 100*(7), 1749e1758.

Khattri, K. N. (1987). Great earthquakes, seismicity gaps and potential for earthquake disaster along the Himalaya plate boundary. *Tectonophysics, 138*(1), 79–92. https://doi.org/10.1016/0040-1951(87)90067-9

Kilaru, S., Goud, B. K., & Rao, V. K. (2013). Crustal structure of the western Indian shield: Model based on regional gravity and magnetic data. *Geoscience Frontiers, 4*(6), 717–728. https://doi.org/10.1016/j.gsf.2013.02.006

Krishna, V. G., & Rao, V. (2011). Velocity modeling of a complex deep crustal structure across the Mesoproterozoic south Delhi Fold Belt, NW India, from joint interpretation of coincident seismic wide-angle and near-offset reflection data: An approach using unusual reflections in wide-angle and near-offset. reflection data. *Journal of Geophysical Research, 116*(1), 1–22. https://doi.org/10.1029/2009JB006660

Kumar, C. R., Raj, A., Pathak, B., Maiti, S., & Naganjaneyulu, K. (2020). High density crustal intrusive bodies beneath Shillong plateau and Indo Burmese Range of northeast India revealed by gravity modeling and earthquake data. *Physics of the Earth and Planetary Interiors, 307*, 106555. https://doi.org/10.1016/j.pepi.2020.106555

Kumar, M. R., Singh, A., Kumar, N., & Sarkar, D. (2015). Passive seismological imaging of the Narmada paleo-rift, central India. *Precambrian Research, 270*, 155–164. https://doi.org/10.1016/j.precamres.2015.09.013

Kumar, S., Gupta, S., Kanna, N., & Sivaram, K. (2020). Crustal structure across the Deccan Volcanic Province and Eastern Dharwar craton in south Indian shield using receiver function modelling. *Physics of the Earth and Planetary Interiors, 306*(June), 106543. https://doi.org/10.1016/j.pepi.2020.106543

Li, A., & Mashele, B. (2009). Crustal Structure in the Pakistan Himalaya from teleseismic receiver functions. *Geochemistry, Geophysics, Geosystems, 10*(12), 1–11. https://doi.org/10.1029/2009GC002700

Liu, M., Yang, Y., Stein, S., Zhu, Y., & Engeln, J. (2000). Crustal shortening in the Andes: Why do GPS rates differ from geological rates? *Geophysical Research Letters, 27*(18), 3005–3008. https://doi.org/10.1029/2000GL008532

Liu, Y., & Rice, J. R. (2005). Aseismic slip transients emerge spontaneously in three-dimensional rate and state modeling of subduction earthquake sequences. *Journal of Geophysical Research, 110*(8), 1–14. https://doi.org/10.1029/2004JB003424

Lysmer, J., & Kuhlemeyer, R. L. (1969). Finite dynamic model for infinite media. *Journal of the Engineering Mechanics Division, 95*(4), 859–877.

Mandal, A., Gupta, S., Mohanty, W. K., & Misra, S. (2015). Subsurface structure of a craton–mobile belt interface: Evidence from geological and gravity studies across the Rengali Province-

Eastern Ghats Belt boundary, eastern India. *Tectonophysics, 662*, 140–152.

Mandal, P. (2006). Sedimentary and crustal structure beneath Kachchh and Saurashtra regions, Gujarat, India. *Physics of the Earth and Planetary Interiors, 155*(3–4), 286–299. https://doi.org/10.1016/j.pepi.2006.01.002

Mandal, P., & Biswas, K. (2016). Teleseismic receiver functions modeling of the eastern Indian craton. *Physics of the Earth and Planetary Interiors, 258*, 1–14. https://doi.org/10.1016/j.pepi.2016.07.002

Manglik, A. (2002). Shear wave velocity structure of the upper mantle under the NW Indian ocean. *Journal of Geodynamics, 34*(5), 615–625. https://doi.org/10.1016/S0264-3707(02)00033-9

Manglik, A., Thiagarajan, S., Mikhailova, A. V., & Rebetsky, Y. (2008). Finite element modelling of elastic intraplate stresses due to heterogeneities in crustal density and mechanical properties for the Jabalpur earthquake region, central India. *Journal of Earth System Science, 117*(2), 103–111. https://doi.org/10.1007/s12040-008-0001-6

Mazumder, S. K. (1976). A summary of the Precambrian geology of the Khasi Hills Meghalaya. *Geological Survey of India, 23*, 311–324.

Mitra, S., Priestley, K. F., Borah, K., & Gaur, V. K. (2018). Crustal structure and evolution of the Eastern Himalayan Plate Boundary system, Northeast India. *Journal of Geophysical Research, 123*(1), 621–640. https://doi.org/10.1002/2017JB014714

Mukhopadhyay, D. (2001). The Archean nucleus of Singhbhum: The present state of knowledge. *Gondwana Research, 4*, 307–318.

Mukhopadhyay, J., Beukes, N. J., Armstrong, R. A., Zimmermann, U., Ghosh, G., & Medda, R. A. (2008). Dating the oldest Greenstone in India: A 3.51 Ga precise U-Pb SHRIMP Zircon Age for Dacitic Lava of the Southern Iron Ore Group Singhbhum Craton. *The Journal of Geology, 116*, 449–461.

Mukul, M. (2000). The geometry and kinematics of the Main Boundary Thrust and related neotectonics in the Darjiling Himalayan fold-and-thrust belt, West Bengal. *India. Journal of Structural Geology, 22*(9), 1261–1283.

Mukul, M. (2010). First-order kinematics of wedge-scale active Himalayan deformation: Insights from Darjiling–Sikkim–Tibet (DaSiT) wedge. *Journal of Asian Earth Sciences, 39*(6), 645–657.

Murty, A. S. N., Tewari, H. C., & Reddy, P. R. (2004). 2-D crustal velocity structure along Hirapur-Mandla profile in central India: An update. *Pure and Applied Geophysics, 161*(1), 165–184. https://doi.org/10.1007/s00024-003-2429-6

Najman, Y., Allen, R., Willett, E. A. F., Carter, A., Barfod, D., Garzanti, E., Wijbrans, J., Bickle, M. J., Vezzoli, G., Ando, S., Oliver, G., & Uddin, M. J. (2012). The record of Himalayan erosion preserved in the sedimentary rocks of the Hatia trough of the Bengal Basin and the Chittagong Hill Tracts Bangladesh. *Basin Research Journal, 24*, 499–519. https://doi.org/10.1111/j.1365-2117.2011.00540.x

Narayanaswami, S., Chakraborty, S. C., Vemban, N. A., Shukla, K. D., Subramanyam, M. R., Venkatesh, V., Rao, G. V., Anandalwar, M. A., & Nagrajaiah, R. A. (1963). The geology and manganese ore deposits of the manganese belts in Madhya Pradesh and adjoining parts of Maharashtra. *Bulletin of the Geological Survey of India Series A, 22*(1), 69p.

Oldham, R. D. (1899). Report on the Great Earthquake of 12th June 1897. *Memoirs of the Geological Survey of India, 29*, 1–379.

Parvez, I. A. (2012). New approaches for seismic hazard studies in the Indian subcontinent. *Geomatics, Natural Hazards and Risk, 4*(4), 299–319. https://doi.org/10.1080/19475705.2012.731659

Pathak, A., Ravi Kumar, M., & Sarkar, D. (2006). Seismic structure of Sri Lanka using receiver function analysis: A comparison with other high-grade Gondwana terrains. *Gondwana Research, 10*(1–2), 198–202. https://doi.org/10.1016/j.gr.2005.10.006

Perfettini, H., Stein, R. S., Simpson, R., & Cocco, M. (1999). Stress transfer by the 1988–1989 M = 5.3 and 5.4 Lake Elsman foreshocks to the Loma Prieta fault: Unclamping at the site of peak mainshock slip. *Journal of Geophysical Research, 104*(9), 20169–20182. https://doi.org/10.1029/1999JB900092

Radhakrishna, B. P. (1989). Suspect tectono-stratigraphic terrane elements in the Indian subcontinent. *Journal of the Geological Society of India, 34*, 1–24.

Rajasekhar, R. P., & Mishra, D. C. (2008). Crustal structure of Bengal Basin and Shillong Plateau: Extension of Eastern Ghat and Satpura Mobile Belts to Himalayan fronts and seismotectonics. *Gondwana Research, 14*(3), 523–534. https://doi.org/10.1016/j.gr.2007.10.009

Ramakrishnan, M. (1988). Tectonic evolution of the Archaean high-grade terrain of South India. *Lunar and Planetary Inst., Workshop on the Deep Continental Crust of South India.*

Rao, C. D., Santosh, M., & Wu, Y. B. (2011). Mesoproterozoic ophiolitic mélange from the SE periphery of the Indian Plate: U-Pb zircon ages and tectonic implications. *Gondwana Research, 19*, 384–401. https://doi.org/10.1016/j.gr.2010.06.007

Rao, S. P., & Tewari, H. C. (2005). The seismic structure of the Saurashtra crust in northwest India and its relationship with the Réunion Plume. *Geophysical Journal International, 160*(1), 319–331. https://doi.org/10.1111/j.1365-246X.2004.02448.x

Rao, V. V., Sain, K., Reddy, P. R., & Mooney, W. D. (2006). Crustal structure and tectonics of the northern part of the Southern Granulite Terrane, India. *Earth and Planetary Science Letters, 251*(1–2), 90–103. https://doi.org/10.1016/j.epsl.2006.08.029

Reddy, P. R. (2003). Deep seismic reflection and refraction/wide-angle reflection studies along Kuppam-Palani transect in the southern granulite terrain of India. *Memoirs of the Geological Survey of India, 50*, 79–106.

Rekha, S., Upadhyay, D., Bhattacharya, A., Kooijman, E., Goon, S., Mahato, S., & Pant, N. C. (2011). With structural and chronological constraints for the tectonic restoration of Proterozoic accretion in the Eastern Indian Precambrian shield. *Precambrian Research, 187*, 313–333.

Sahoo D. (2012). Neotectonics- active tectonics of frontal Siwalik range and Soan dun in Himachal Pradesh, NW Himalaya. D. Phil thesis H N B Garhwal University Srinagar, p. 149.

Sahu, V. K., Gahalaut, V. K., Rajput, S., Chadha, R. K., Laishram, S. S., & Kumar, A. (2006). Crustal deformation in the Indo-Burmese arc region: Implications from the Myanmar and Southeast Asia GPS measurements. *Current Science, 90*(12), 1688–1693. http://www.jstor.org/stable/24091921.

Sahu, S., Saha, D., & Dayal, S. (2015). Sone megafan: A non-Himalayan megafan of craton origin on the southern margin of the middle Ganga Basin, India. *Geomorphology, 250*, 349–369.

Saikia, S., Baruah, S., Chopra, S., Gogoi, B., Singh, U. K., & Bharali, B. (2019). An appraisal of crustal structure of the Indo-Burmese subduction region. *Journal of Geodynamics, 127*, 16–30.

Salomon, C. (2018). Finite element modelling of the geodynamic processes of the Central Andes subduction zone: A reference model. *Geodesy and Geodynamics, 9*(3), 246–251. https://doi.org/10.1016/j.geog.2017.11.007

Santosh, M. (1996). The Trivandrum and Nagercoil blocks. In M. Santosh & M. Yoshida (Eds.), *The Archaean and Proterozoic Terrains of Southern India within Gondwana. Gondwana research* (pp. 243–277). Field Science Publications.

Satyavani, N., Dixit, M. M., & Reddy, P. R. (2001). Crustal velocity structure along the Nagaur-Rian sector of the Aravalli fold belt, India, using reflection data. *Journal of Geodynamics, 31*(4), 429–432. https://doi.org/10.1016/S0264-3707(01)00004-7

Scholz, C. H., & Campos, J. (1995). On the mechanism of seismic decoupling and back arc spreading at subduction zones. *Journal of Geophysical Research.* https://doi.org/10.1029/95jb01869

Seeber, L., Armbruster, J., Simpson, D. W., & Richards, P. G. (1981). *Earthquake prediction: An international review* (p. 259). American Geophysical Union.

Sharma, A., Baruah, S., Piccinini, D., Saikia, S., Phukan, M. K., Chetia, M., & Kayal, J. R. (2017). Crustal seismic anisotropy beneath Shillong plateau-Assam valley in North East India: Shear-wave splitting analysis using local earthquakes. *Tectonophysics, 717*(June), 425–432. https://doi.org/10.1016/j.tecto.2017.08.027

Sharma, R. S. (2011). *Cratons and Fold Belts of India.* Springer. https://doi.org/10.1007/978-3-642-01459-8

Shemenda, A. I., & Grocholsky, A. L. (1992). Physical modelling of lithosphere subduction in collision zones. *Tectonophysics, 216*(3–4), 273–290. https://doi.org/10.1016/0040-1951(92)90401-Q

Singh, A. P. (1999). The deep crustal accretion beneath the Laxmi Ridge in the northeastern Arabian Sea: The plume model again. *Journal of Geodynamics, 27*(4–5), 609–622. https://doi.org/10.1016/S0264-3707(98)00019-2

Singh, A., Bhushan, K., Singh, C., Steckler, M. S., Akhter, S. H., Seeber, L., & Biswas, R. (2016). Crustal structure and tectonics of Bangladesh: New constraints from inversion of receiver functions. *Tectonophysics, 680*, 99–112. https://doi.org/10.1016/j.tecto.2016.04.046

Singh, A. P., Kumar, N., & Singh, B. (2006). Nature of the crust along Kuppam-Palani geotransect (South India) from Gravity studies: Implications for Precambrian continental collision and delamination. *Gondwana Research, 10*(1–2), 41–47. https://doi.org/10.1016/j.gr.2005.11.013

Singh, A. P., Mishra, D. C., Gupta, S. B., & Rao, M. R. K. P. (2004b). Crustal structure and domain tectonics of the Dharwar Craton (India): Insight from new gravity data. *Journal of Asian Earth Sciences, 23*(1), 141–152. https://doi.org/10.1016/S1367-9120(03)00115-9

Singh, A., & Singh, C. (2019). Seismic imaging of the deep crustal structure beneath Eastern Ghats Mobile Belt (India): Crustal growth in the context of assembly of Rodinia and Gondwana supercontinents. *Precambrian Research, 331*, 105343. https://doi.org/10.1016/j.precamres.2019.105343

Singh, D. D. (1988). Crust and upper-mantle velocity structure beneath the northern and central Indian Ocean from the phase and group velocity of Rayleigh and Love waves. *Physics of the Earth and Planetary Interiors, 50*(3), 230–239. https://doi.org/10.1016/0031-9201(88)90104-5

Singh, V. P., & Shanker, D. (1993). Flow of Tibetan Plateau and tectonic along Burmese Arc. *Geophysical Transactions, 38*(2–3), 135–149.

Singh, V. P., Shanker, D., & Singh, R. (2004a). A structural and tectonic synthesis of parts of Archeans, Satpuras and Chhattisgarh basins around Mandala-Raipur districts, M. P. India, using gravity field data. *IUGG Special Volume' Earthquake Hazard, Risk, and Strong Ground Motion, 1*, 121–136.

Singh, V. P., Singh, C. L., & Shanker, D. (1995). Patna fault as a subsurface feature of the Ganga-Basin and its geodynamic constraints. *Proc. Indian National Science Academy, 61A*(1), 47–52.

Sinha, R., Kettanah, Y., Gibling, M. R., Tandon, S. K., Jain, M., Bhattacharjee, P. S., Dasgupta, A. S., & Ghazanfari, P. (2009). Craton-derived alluvium as a major sediment source in the Himalayan foreland basin of India. *Geological Society of America Bulletin, 121*, 1596–1610.

Sinha, R., Tandon, S., Gibling, M., Bhattacharjee, P., & Dasgupta, A. (2005). Late Quaternary geology and alluvial stratigraphy of the Ganga Basin. *Himalayan Geology, 26*(1), 223–240.

Sinha-Roy, S., Malhotra, G., & Mohanty, M. (1998). *Geology of Rajasthan.* Bangalore: Geological Society of India.

Sitharam, T. G., & Kolathayar, S. (2013). Seismic hazard analysis of India using areal sources. *Journal of Asian Earth Sciences, 62*, 647–653.

Srivastava, V., Mukul, M., & Mukul, M. (2017). Quaternary deformation in the Gorubathan recess: Insights on the structural and landscape evolution in the frontal Darjiling Himalaya. *Quaternary International, 462*, 138–161.

Steckler, M. S., Mondal, D. R., Akhter, S. H., Seeber, L., Feng, L., Gale, J., Hill, E. M., & Howe, M. (2016). Locked and loading megathrust linked to active subduction beneath the Indo-Burman ranges. *Nature Geoscience.* https://doi.org/10.1038/ngeo2760

Stein, R. S., King, G. C., & Lin, J. (1994). Stress Triggering of the 1994 M = 67 Northridge, California earthquake by its predecessors. *Science, 265*(5177), 1432–1435. https://doi.org/10.1126/science.265.5177.1432

Suito, H., Iizuka, M., & Hirahara, K. (2002). 3-D viscoelastic FEM modeling of crustal deformation in northeast Japan. *Pure and Applied Geophysics, 159*(10), 2239–2259. https://doi.org/10.1007/s00024-002-8733-8

Tandon, A. N. (1959). The Rann of Cutch earthquake of 21 July 1956. *Indian Journal of Meteorology and Geophysics, 10*, 137–146.

Thakur, V. C. (2013). Active tectonics of Himalayan Frontal Fault system. *Int J Earth Sci (geol Rundsch), 102*, 1791–1810. https://doi.org/10.1007/s00531-013-0891-7

Tiwari, R. P. (2010). Status of Seismicity in the Northeast India and Earthquake Disaster Mitigation. *ParvezENVIS Bulletin, 10*(1), 114.

Tiwari, V. M., Rao, M. V., & Mishra, D. C. (2001). Density inhomogeneities beneath Deccan Volcanic Province, India as derived from gravity data. *Journal of Geodynamics, 31*(1), 1–17.

Turcotte, D. L., & Schubert, G. (2002). *Geodynamics (second).* Cambridge University.

Wang, K., He, J., Dragert, H., & James, T. S. (2001). Three-dimensional viscoelastic interseismic deformation model for the Cascadia subduction zone. *Earth, Planets and Space, 53*(4), 295–306. https://doi.org/10.1186/BF03352386

Wiens, D. A., DeMets, C., Gordon, R. G., Stein, S., Argus, D., Engeln, J. F., & Woods, D. F. (1985). A diffuse plate boundary

model for Indian Ocean tectonics. *Geophysical Research Letters, 12*(7), 429–432.

Yeats, R. S., & Thakur, V. C. (2008). Active faulting south of the Himalayan front: Establishing a new plate boundary. *Tectonophysics*, *453*, 63–73.

Zhao, S., Müller, R. D., Takahashi, Y., & Kaneda, Y. (2004). 3-D finite-element modelling of deformation and stress associated with faulting: Effect of inhomogeneous crustal structures.

Geophysical Journal International, 157(2), 629–644. https://doi.org/10.1111/j.1365-246X.2004.02200.x

Zoback, M. L., Zoback, M. D., Adams, J., Assumpcao, M., Bell, S., Bergman, E. A., Bluemling, P., Brereton, N. R., Denham, J., Ding, J., Fuchs, K., Gay, N., Gregersen, S., Gupta, H. K., Gvishani, A., Jacob, K., Klein, R., Knoll, P., Magee, M., … Zhizhin, M. (1989). Global patterns of tectonic stress. *Nature, 341*, 291–298.